Central volcanoes and caldera collapses in the late Miocene – late Pleistocene Tibesti Volcanic Province, northwest Chad

Abdelsalam Elshaafi[1], Agust Gudmundsson[2]

[1]Department of Earth Sciences, Faculty of Science, University of Benghazi, Libya
[2]Department of Earth Sciences, Royal Holloway University of London, Egham TW20 0EX, UK (abdelsalamelshaafi@yahoo.co.uk; a.gudmundsson@rhul.ac.uk)

Abstract

The Tibesti Volcanic Province (TVP) in northwest Chad represents the second largest of the five Gharyan–Tibesti volcanic provinces and covers an area around 29,000 km^2. The other four provinces are in Libya, but all five provinces are from late Miocene to Quaternary and may have a common mantle source. The TVP, however, differs from the other four as regards volcano-tectonic processes, eruption style, and production of volcanic materials. The volcanic products of the TVP were erupted from the end of Miocene to late Pleistocene, range from basaltic to acidic, and suggest a double magma source – a shallow chamber fed by a deeper and larger reservoir. More specifically, field observations and numerical modelling results suggest that the basaltic magmas forming scoria cones, primarily at the periphery of the TVP, came from a deeper magma reservoir in the lower crust while the rhyolite and ignimbrites were fed by a shallow crustal magma chamber. By contrast, the volcanic products of the four volcanic provinces in Libya are primarily basalts and fed directly from single deep reservoirs. In the period from 8 Ma to 7-5 Ma, the evolution of the TVP was characterised by the formation of central volcanoes. Subsequently, in the period from 7-5 Ma to 0.43 Ma, the TVP was subject to caldera collapses that produced large-volume ignimbrites (>100 km^3). Here we present numerical models with plausible loading conditions to understand better the volcano-tectonic evolution of the TVP and the spatial and temporal distribution of its major volcanic units. Our results suggest that the normal local stress field encouraged the formation of a central-volcano edifice (a volcanic cone) fed by radial dykes and inclined sheets and mostly erupting small volumes. By contrast, stress fields generated as a result of small crustal uplift or doming, due to the accumulation of

magma in a deep-seated reservoir, triggered the formation of a ring-fault and the injection of a ring-dyke above the lateral margins of a shallow crustal magma chamber. Subsequently, the piston-like caldera subsidence helped to squeeze magma out of the shallow chamber resulting in large eruptions.

Keywords: Volcanotectonics, Magma chamber, Magma reservoir, Caldera collapse, Chad volcanism, Libya volcanism

1 Introduction

The Tibesti Massif (or the Tibesti Mountains), with an area of about 100,000 km^2, is located in the central Sahara desert, mostly in northwestern Chad but extends into northeastern Niger and southern Libya (Permenter and Oppenheimer 2007; Deniel et al., 2015)(Fig. 1a). The Massif is a dome with elevations in excess of 3,000 m, and its southern part contains a volcanic field, of late Miocene to late Pleistocene age, with an area of around 29,000 km^2. The Tibesti Volcanic Province (TVP), located in northwestern Chad, is the southernmost of the five main volcanic provinces of similar age in this part of Africa, four of which are in Libya. From north to south, the five provinces are (Fig. 1) the Gharyan Volcanic Province (GVP), the As Sawda Volcanic Province (SVP), the Al Haruj Volcanic Province (AHVP), the Nuqay Volcanic Province (NVP), and the Tibesti Volcanic Province (TVP) (Bardintzeff et al., 2012; Elshaafi and Gudmundsson, 2016; Ball et al., 2019). These five volcanic fields represent the Neogene–Quaternary outpouring of volcanic activity and cover a total area of about 95,000 km^2 (Fig. 1a). The lava flows of four provinces in Libya are primarily alkali to transitional basaltic rocks - with a minor amount of phonolites and trachyte only in GVP and NVP (e.g., Staurt et al., 2014; Radivojević et al., 2015; Ball et al., 2019). By contrast, the surface of TVP is mostly composed of trachyte trachyte/andesite ignimbrites and lava flows, as well as basaltic lava flows (Gourgaud and Vincent, 2004; Deniel et al., 2015).

The five Tibesti–Gharyan volcanic provinces are spatially related to two main structural zones. One strikes NW-SE to NNW-SSE and is composed of early Palaeozoic structural elements, the other strikes ENE-WSW and is composed of late Palaeozoic to Mesozoic structural elements (Hercynian Orogeny) (Fig. 1a) (Woller and Fediuk, 1980; Lemnifi et al., 2019). These conjugate zones of regional elements

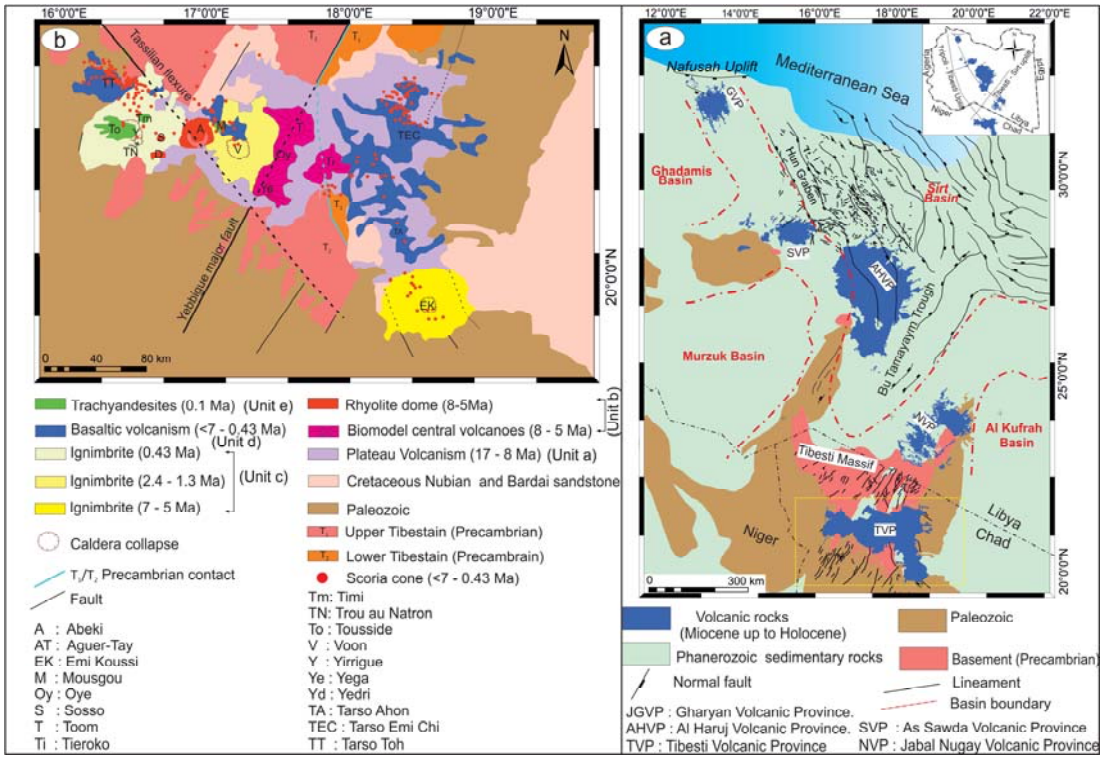

Figure 1. a) Simplified geological map showing the distribution of the main Tibesti – Gharyan volcanic provinces which are generally arranged NW-SE direction (modified from Abadi et al., 2008; Deniel et al., 2015). The inset map shows the main orthogonal pre-existing structural trends based on Woller and Fediuck (1980). The dashed orange box shows the location of Fig. 1b. b) Volcanotectonic map of the Tibesti Volcanic Province showing the distribution of the five main volcanic units and the tectonic framework. Three collapse calderas are indicated by yellow colours with associated large volume of ignimbrites (> 100km^3) that are aligned with an NW-SE linear trend. Three bimodal central volcanoes are marked by pink colour and a NE-SW trend along Yebbigue major fault. Scoria cones are indicated by red spots and mainly concentrated at the margin of province as well as around collapse calderas. The Precambrian rocks were divided into the Lower Tibestain (T1) and Upper Tibestain (T2) (modified from Permenter and Oppenheimer, 2007; Deniel et al., 2015).

are likely to be inherited from the previous structural zones in the basement and have played a significant role in the geological evolution of the North Africa (Woller and Fediuk, 1980). The main volcanic provinces in North Africa occur at intersections between these ancient basement zones, which also control the boundaries of the main sedimentary basins (Fig. 1a). More specifically, these intersections, some with exposed Precambrian rocks, seem to have encouraged the generation of volcanic provinces during the Neogene to Quaternary period (Vail, 1971;Busrewil and Oun, 1991; Goudarzi, 1980; El-Makhrouf, 1988; Less et al., 2006; Lemnifi et al., 2017, 2019).

While the main volcanotectonic elements of the above four volcanic provinces in Libya are reasonably well known, those of the Tibesti Volcanic Province (TVP) in Chad are, as indicated above, still poorly known. One main aim of the present paper is thus to describe the volcanotectonics of the TVP (Fig. 1) so as to make a more detailed comparison with the other four provinces possible. For this purpose, we first provide a general geological and tectonic setting of the TVP. The products and structures generated by the volcanotectonic activity are described, including the main volcanoes. The focus is then in particular on the most spectacular structures of the province, namely three major collapse calderas. These are the calderas of Yirrigue,Voon, and Emi Koussi (Fig. 2). We provide analytical and numerical models to explain the formation of the collapse calderas and put these models in general context of volcanotectonic evolution of central (polygenetic) volcanoes.

2 Geological and tectonic setting

2.1 Volcanotectonics of North Africa

The Neogene to Quaternary volcanic activity in North Africa is extensive, reflects changes in the regional stress fields, and is, presumably, related to mantle convection (Cloetingh and VanWees, 2005; Abadi et. al., 2008). While mantle plumes are widely regarded as the main cause of the flood-basalt volcanism (Wilson and Guiraud, 1998; Abadi et. al., 2008), many models have been suggested for the volcanism of North Africa. For example, Bardintzeff et al. (2012) suggest that part of the volcanisms may be related to reactivation of pre-existing regional basement faults and asthenospheric upwelling (cf. Peregi et al, 2003; Permenter and Oppenheimer, 2007). Burke (1996) suggests mantle plumes caused the doming or swelling of the African plate at the location of the volcanic provinces, while the results of Lie´geois et al. (2005) suggest that the shallow mantle is at least warmer at 80 to 150 km beneath the volcanic provinces which is also indicated by Lemnifi et al. (2019) who suggest the warm mantle may extend to depths of more than 400 km. Other plume or upwelling models for North Africa include those of Keppie et al. (2011), Nixon et al. (2011), and Ball et al. (2019), some of which propose an analogy with the Afar plume (Ebinger and Sleep, 1998; Begg et al., 2009). In particular, Gourgaud and Vincent (2004) suggest a mantle plume beneath the TVP.

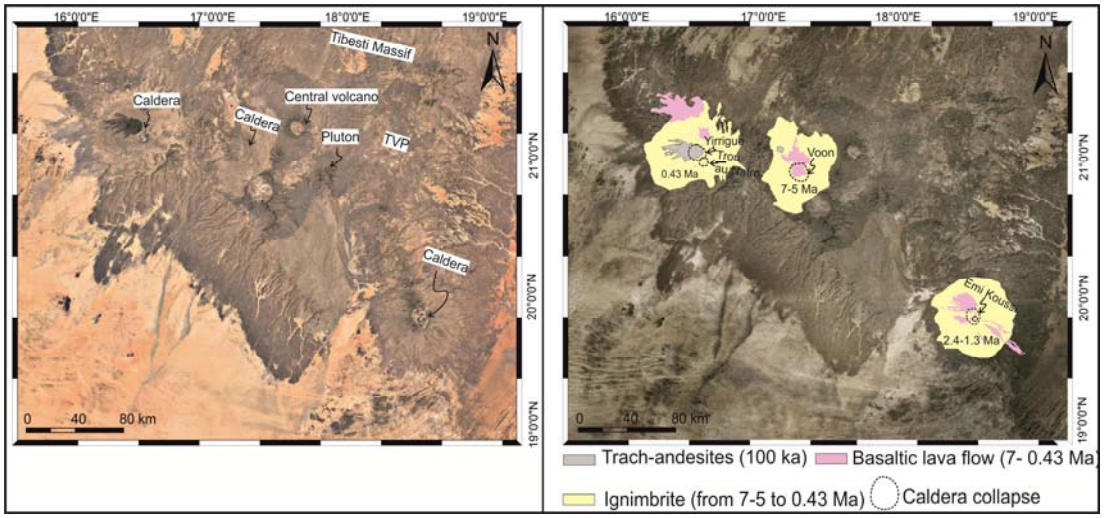

Figure 2. Satellite imagery (adapted from Google Earth) shows the locations of three collapse calderas and the central volcanoes (left image) of the TVP. Note each large ignimbrite eruption (indicated by yellow colour) was followed by the eruption of basaltic and andesitic-trachyte materials (indicated by pink and gray colours, respectively). Yellow colours represent the area covering by ignimbrite and have been estimated by ArcGIS 10.1 as follows: Yirrigue Caldera 3,223 km^2, Emi Koussi Caldera 2,777 km^2 and Voon Caldera 2,167 km^2.

As indicated above, the major volcanic fields in North Africa are strongly correlated with areas of elevated basement. The basement highs presumably reflect some form of subcrustal arching or swelling where magma might have preferentially accumulated to form reservoirs and, subsequently, propagated through dykes to the surface. Thick sedimentary sequences, however, may have acted as sort of barriers between the main volcanic provinces(Vail, 1971, Elshaafi and Gudmundsson, 2017). The Tibesti–Gharyan volcanic provinces are primarily located at the boundary between Neoproterozoic high-grade metamorphic rocks to the east and Neoproterozoic-Palaeozoic low-grade rocks to the west (El-Makhrouf, 1988; Keppie et al., 2011). Schafer et al. (1980) suggest that the general volcanic trend NW–SE is related to the Cretaceous boundary between the NW and SE African subplates which was reactivated during the late Miocene due to the convergence between Africa and Europe (Bardintzeff et al., 2012).

2.2 General structure of the Tibesti Volcanic Province

Although the Tibesti Volcanic Province (TVP) is the second largest of the Tibesti–Gharyan volcanic provinces, it has been poorly studied, partly because of series of sporadic military clashes and conflicts in the area from the 1970s, making fieldwork

extremely challenging and hazardous. Most of the literature is therefore from the early 1950s to the 1970s. For example, Wacrenier et al. (1958) made the first geological map of the Tibesti Massif, while Vincent (1960, 1963, and 1970) provided data on the geology and structure of the massif. From remote-sensing data, Malin (1977) suggested a similarity between the volcanoes on Mars and those of the TVP and, due to slow plate motions of Africa, that the sources of magma for TVP (and the other four provinces) would be essentially stationary relative to the surface. Some more recent studies of the TVP include those by Guiraud et al.(2000), Gourgaud and Vincent (2004), Permenter and Oppenheimer (2007), and Deniel et al. (2015). The details of the structural features, geological history, including post-orogenic magmatism, and principal volcanic units of the TVP are given by Klitzch, (2000), Peregi et al. (2003), and Deniel et al. (2015).

Of relevance here is that the Caledonian orogeny was accompanied by the formation of the NW–SE striking structures, some several hundred kilometres long, such as Tripoli–Tibesti Uplift that is subparallel to the Al Haruj Uplift. The TVP is also influenced by conjugate structures, striking NE-SW to ENE-WSW, formed during the Hercynian orogeny (late Jurassic to early Cretaceous) and were superimposed on the earlier Pan-African system (Fig. 1a). The NE–SW striking Sirt–Tibesti uplift (Sirt Arc) formed during this period. The elevated Precambrian of central Sahara was actively eroded during the Palaeozoic and produced a large volume of clastic materials (Peregi et al., 2003; Fig. 1a). Deniel et al. (2015) suggest that the volcanotectonics of the TVP was influenced by two lineaments, namely, the great NW–SE striking Tassilian flexure to the southwest of the TVP and a major NE–NNE striking Yebbigue fault zone to the east of TVP (Fig. 1b).

2.3 **Volcanic units of the Tibesti Volcanic Province**

In the southern part of the Tibesti mountains, there is a large volume of late Miocene to late Pleistocene volcanic rocks that belong to the TVP. Based on field relationships and volcanological, geochronological, and petrological data, these rocks can be divided into five main volcanic units as follows (Deniel et al., 2015).

(a) The first (oldest) unit was generated by plateau volcanism (17-8 Ma) and consists of alkaline olivine basalts covering some 29,000 km^2 and including several trachytic to phonolite plugs (Fig. 1b). This volcanic unit, which represents the oldest volcanic

rocks in the TVP, was contemporaneous with basaltic lavas of the As Sawda Volcanic Province (SVP), central Libya, which have been dated at between 16 and 8 Ma (Ade-Hall et al. 1974; Woller and Fediuk 1980; Bardintzeff et al., 2012). The plateau volcanism on the TVP was episodic, as indicated by sedimentary layers between lava flows.

(b) The second unit, which extends towards central part of the province, was erupted at the end of Miocene (between 8 and 5 Ma) and forms four large compositionally bimodal central (polygenetic) volcanoes, namely, Yega, Oye, Toom, and Tieroko (Fig. 1b). These central volcanoes are exposed over an area of about 2,700 km^2 and form an eroded plateau. Each central volcano formed in two distinct stages. The first stage consists mainly of basaltic lava created at the margins while the second stage consists mainly of rhyolite lava flows that form the central cores of the volcanoes (Deniel et al., 2015).

(c) The third unit is characterised by multiple caldera collapses. Three major caldera collapses produced three large ignimbrites, of volumes as great as 100 km^3, namely the Voon caldera (7–5 Ma), the Emi Koussi caldera (2.4–1.33 Ma), and Yirrigue caldera (0.43 Ma) (Deniel et al.,2015). Each major caldera collapse coincided with termination of rhyolite production and the initiation of mafic volcanism at and around the caldera ring-fault. Subsequently, the focus of further rhyolite/ignimbrite eruptions migrated to other parts (away from the calderas) of the Tibesti region. This shifting in focus may be partly due the local stress field around the old collapsed magma chambers no longer being favourable for receiving magma from a deeper magma source reservoir (cf. Marti and Gudmundsson, 2000); a new magma chamber (producing rhyolite) may then be formed to either or both sides of the old, collapsed chamber (Fig. 2). We explore this shifting mechanism in more detail in the Discussion.

(d) The fourth unit was formed by basaltic volcanism during the period 7–5 Ma which produced scoria pyroclastic cones and basaltic lavas. The fourth unit is of a similar age and composition as the first volcanic phase at the Haruj Volcanic Province (AHVP) which has been dated at7 Ma to 3.6 Ma (Less et al.,2006; Bardintzeff et al., 2012). Some of the basaltic lavas erupted during the formation of the fourth unit occur along the ring-faults or in the interiors of the three main calderas.

(e) The fifth and most recent volcanic unit to form on the TVP occurs at a rim of Yirrigue caldera in the Tarso Tosside Volcanic Complex and is composed of andesitic trachyte (100 ka). This volcanism as well as Tarso Tousside and Emi Koussi fumarole indicate that the complex is still potentially volcanically active (www.volcano.si.edu) (Permenter and Oppenheimer, 2007). The distribution of the main volcanic units on the TVP given in Fig. (1b) is only a general guideline to the TVP which includes different types of volcano-tectonic elements and associated volcanic events (cf. Deniel et al. 2015).

In the present study, the main volcanic units were examined in detail using ArcGIS 10.1 and multi-source high resolution remote sensing images, such as the satellite imagery available on Google Earth (2016) for the central Sahara desert. Digital elevation model (DEM) and data collected by the NASA Shutter Radar Topography Mission (SRTM) were also used. Google Earth imagery provides three-dimensional geospatial data through Keyhole Mark-up Language (KML). The images of TVP provide a high-resolution of about 0.5–2.5 m and are considerably enhanced by the extremely good preservation of volcanic features because of the aridity of the region (Permenter and Oppenheimer, 2007; Abdunaser and McCaffrey, 2014). The images thus make it possible to measure accurately for example the geometry of volcanoes and the azimuth and thickness of inclined sheets and dykes. The present work confirms that high-resolution remote sensing is an effective and efficient complementary tool to traditional volcanotectonic field measurements, particularly in arid and remote and hazardous regions (cf. Drury, 2001; Rajesh, 2004; Permenter and Oppenheimer, 2007; Chen et al., 2014; Abdunaser and McCaffrey, 2014). The geometry of each volcanic unit is defined by its length, width (diameter), area, volume, and depth or thickness. ArcGlobe 10.1 was used to plot the scoria cones, then the shape files of scoria cones imported into ArcMap10.1 that were added to the map through georeferenced raster images of the geological maps of the TVP prepared by Permenter and Oppenheimer(2007); Deniel et al. (2015) as a baseline (Fig. 1a, b).

We provide a model where the formation of the main central volcanoes and, the subsequently generated, collapse calderas are both the consequence of the existence of a shallow magma chamber. Finite element methods (FEM) are used to calculate the local stress fields associated with magma chambers to better understand the

volcanotectonics of the formation of central volcanoes and collapse calderas. A magma chamber is modelled as a hole within the Earth's crust subject to three primary loading conditions, namely: (i) excess magmatic pressure (pressure above lithostatic) within the magma chamber, (ii) tensile stresses generated by regional lateral extension (due to rifting or/and spreading), and (iii) compressive stress at the bottom of the crust during the end of Miocene due to accumulation magma that caused regional doming or uplift. The results indicate that doming of the lower margin (bottom) of crust played a major role in generating the three major calderas (ring-fault formation) while excess magmatic pressure in the chamber and far-field extension favoured construction of the central volcanoes (through the injection of radial dykes and inclined sheets).

The evolution of the TVP is characterised by primarily a volcano-forming constructive period (between 8 and 7-5 Ma), and then a caldera-collapse destructive period (between 7–5 and 0.43 Ma). The constructive period involved the accumulation of volcanic materials for formation of polygenetic (central) volcanoes (volcanic unit b) whereas the destructive period involved vertical caldera collapses and the production of large volumes of ignimbrites (volcanic unit c). In-between the ignimbrite eruptions, the caldera activity was characterised by widespread basaltic to andesitic-trachyte volcanism. Similar activity patterns have been observed in many collapse calderas worldwide, for instance in the Las Canada caldera in Tenerife (Marti and Gudmundsson, 2000).

Stratigraphic and geochronological data show that during the development of the calderas the focus of felsic volcanic activity migrated with time from the centre of the volcanic province at the Voon caldera (7-5 Ma) to the southwest part of the province, at the Emi Koussi caldera (2.4–0.33 Ma), and then finally to the northeast part, at the Yirrigue caldera (0.43 Ma) (Fig. 2). The conceptual analogue and analytical modelling of the development of the overlapping collapse calderas of Las Canadas, Tenerife (Canary Islands), generated by magma-chamber migration, appears to be applicable to the TVP - although the calderas of the TVP are separate rather than overlapping (Fig. 13). The dimensions (diameters), areas, maximum depths (visible ring-fault displacements), and ignimbrite volumes of the three calderas of the TVP are summarised in Table 1. The eruptive volumes, estimated by Deniel et al. (2015), are a crude measure of the magma volumes that left the magma

chamber during eruption. When the volumes of the pyroclastic materials have been reduced to dense-rock-equivalents (DRE), then the eruptive volumes may be regarded as minimum estimates for the corresponding magma volumes leaving the chamber because of subsequent erosion and burial of parts many of the eruptive units.

In contrast to the single-magma sources of the volcanic provinces in Libya, the volcanoes of the TVP are likely to be fed by double magma chambers (Fig.3a). Then the shallow magma chamber is located within the upper crust and produced the more evolved products while also erupting mafic magmas. By contrast, the deeper magma chamber (the magma reservoir) is presumably located in the lower crust or at the crust-mantle boundary and produced primarily mafic (primitive) eruptives, mainly basaltic lava flows. Here we focus first on the conditions for rupture of the shallow upper chamber and resulting dyke or inclined sheet emplacement.

3 Conditions for magma chamber rupture and dyke emplacement

A shallow crustal magma chamber is normally active over a considerable period of time, commonly $10^{4\text{-}6}$years. The chamber may develop from an original sill which absorbs the magma of many dykes whilst it is still liquid and thereby grows in size or, alternatively, from many smaller sills that merge into a large one (e.g., Karlstrom et al., 2017; Gudmundsson, 2020). The rate of growth of chambers, as well as their rupture and dyke-injection frequencies, vary widely (e.g. Pinel and Jaupart, 2004; Karlstrom et al., 2010; Maccaferri et al., 2011; Gudmundsson, 2020). Once the chamber ruptures, dyke or, depending on the local stress field, inclined sheet injection occurs. The subsequent propagation of the resulting dyke/sheet has been studied by many (e.g. Dahm, 2000; Pinel and Jaupart, 2004; Maccaferri et al., 2011, Rivalta et al., 2015; Townsend et al., 2017). Here, however, the main focus is on the rupture of the chamber.

The condition for rupture of a magma chamber and emplacement of a dyke or an inclined sheet is (Gudmundsson, 2020):

$$p_l + p_e = \sigma_3 + T_0 \qquad (1)$$

where p_l is the lithostatic pressure, p_e is the magmatic excess pressure (pressure above the lithostatic pressure) in the magma chamber prior to rupture and dyke emplacement, and T_0 is the tensile strength of the host rock in the roof and the walls of the chamber. Furthermore, σ_3 denotes the minimum compressive (maximum tensile) principal stress, here is given by its absolute value (positive), which is normally perpendicular to the propagation path of the dyke/sheet. Most magma chambers rupture only infrequently in comparison with their lifetimes and are thus commonly in an lithostatic equilibrium with host rock so that $\sigma_3 = \sigma_2 = p_t = \sigma_1$ (that is, minimum, intermediate, and maximum principal compressive stresses, σ_3, σ_2 and σ_1 are equal to the total magmatic pressure p_t) and the excess pressure p_e is zero. During an unrest period, however, the excess pressure p_e in the chamber becomes positive and when the condition $p_e = T_0$ is satisfied the chamber ruptures and injects a dyke/sheet. This condition can be reached through (i) magma replenishment from the deeper source chamber/reservoir, (ii) gas exsolution from the magma, or (iii) reduction in σ_3 during tectonic-driven extension. The in-situ tensile strength T_0 of rocks is in range 0.5 to 9 MPa, the most common values being 2–4 MPa (Haimson and Rummel, 1982; Amadei and Stephansson, 1997). In all the numerical models we use the excess magmatic pressure 5 MPa as a reasonable value at chamber rupture.

Once a magma chamber ruptures the magmatic overpressure (driving or net pressure) forms a fluid-driven fracture, namely a magma-filled extension fractures that, subsequently, crystallises to form a sheet intrusion (Tibaldi, 2015; Gudmundsson, 2020).We consider a vertical dyke to illustrate the mechanical principles involved. Following magma-chamber rupture and as the dyke begins to propagate up into the roof of the chamber, the magmatic overpressure in the dyke is given by (Kusumoto et al., 2013):

$$p_o = p_e + (\rho_r - \rho_m)gh + \sigma_d \qquad (2)$$

where ρ_r is the average density of the crustal layers which the dyke dissects, ρ_m is the magma density (assumed constant), g is acceleration due to gravity (assumed constant), h is the dyke dip dimension above magma chamber and σ_d is the

differential stress at the level where the dyke is observed..The magmatic overpressure p_0 measures the difference between the total magmatic pressure and minimum compressive (maximum tensile) principal stress σ_3, which generally acts normal to the dyke. The overpressure of the magma in the dyke on its path towards the surface increases so long as the buoyancy term $(\rho_r - \rho_m)gh$ is positive. During fissure eruptions, the overpressure p_0 has a large effect on the effusion rate (Kusumoto et al., 2013). The feeder-dyke overpressure at the Al Haruj Volcanic Province, central Libya, has been estimated at 8–19 MPa (Elshaafi and Gudmundsson, 2016), even though the excess magmatic pressure in the chamber normally does not exceed the in-situ tensile strength, so is normally about 5 MPa or less, as indicated above. The comparatively high dyke overpressure is due to positive buoyancy, which adds to the overpressure (Eq. 2).

The majority of dykes injected from magma chambers become arrested or deflected into sills at various levels of the Earth's crust (e.g. Dahm, 2000; Maccaferri et al., 2011; Browning et al., 2015). Dyke arrest or deflection into sill is due to three main mechanisms, namely :i) Stress barriers (layers where the principals stresses have turned so as to become unsuitable to dyke emplacement . ii) The Cook-Gordon debonding or delamination (induced dyke-parallel tensile stress opens the contact ahead of the propagating dyke tip). iii) Elastic mismatch mechanism (relates to abrupt change in Young's modulus across a contact in relation to the contact properties and material toughness). Further details of the arrest and deflection of dykes are given by Browning and Gudmundsson (2015), Elshaafi and Gudmundsson (2016), and Gudmundsson (2020).

4 Mechanism of constructive central volcanoes

4.1 Magma-chamber geometry

Field observations and geophysical studies suggest that the geometry of long-lived magma chambers approaches the ideal ellipsoidal or spherical shape rather than being irregular, particularly during the later stages of their evolutions (Gautenb et al., 1989; Acocella, 2007). The vertical cross-section of many magma chambers may thus be assumed to be circular. For a chamber with a circular geometry at depth (d)

and radius r and subject to an internal magmatic excess pressure p_e (Fig. 3b), the tensile stress associated with magma chamber is given by (Savin, 1961):

$$\sigma_b = p_e(1 + 2\tan 2\theta) \quad (3)$$

where σ_b is the tensile stress along the boundary of the chamber and θ is the angle between the vertical axis and tangent (AZ) to the boundary of the magma chamber. The maximum tensile stress occurs at the both sides (c_1 and c_2) of the chamber where the angle reaches a maximum at these points. On the top of the chamber at point b the tensile stress is equal to magmatic excess pressure p_e. The maximum tensile stresses σ_{max} at points c_1 and c_2 occurs when the radius r of chamber is close to the depth d of the magma chamber and can be found from (Gudmundsson, 1998) (Fig. 3b);

$$\sigma_{max} = \frac{p_e(d^2 + r^2)}{(d^2 - r^2)} \quad (4)$$

All symbols are as defined above. When d is > 1.73 r, the maximum tensile stresses at both sides of chambers at points c_1 and c_2 is greater than maximum tensile stress at the free surface above magma chamber at point a.

Deep erosion in parts of the TVP, probably reaching several kilometres below the original surface in places (Vincent 1970; Deniel et al., 2015) particularly in the extinct central volcano Tieroko, provide excellent outcrops for understanding the three-dimensional structure and dyke-intrusion paths of the active magma chambers (Fig. 4a). Extinct crustal magma chambers of different sizes, geometries, and depths occur in deeply eroded volcanic regions and are commonly associated with swarms of inclined sheets, radial dykes, ring faults, and ring dykes such as in Iceland and Scotland (Upton, 2004; Gudmundsson, 2020). Swarms of inclined sheets and radial dykes occur in the flanks of the Tieroko volcano and can be traced to a pluton (cf. Deniel et al., 2015), which is probably the uppermost part of extinct or fossil magma chamber (Fig. 4a). Some of the inclined sheets seem to be arrested at various levels, the arrest being primarily through the three mechanisms discussed above (Fig. 5a).

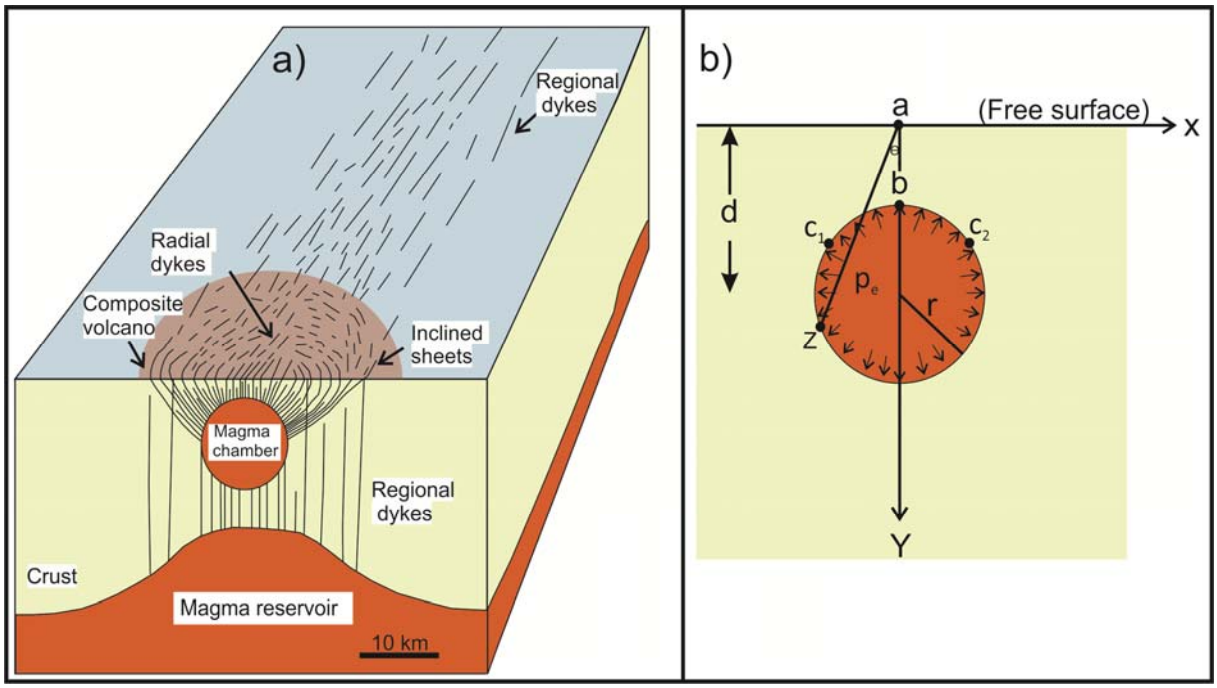

Figure 3. a) Schematic illustration as to how the volcanic field may be fed by double magma sources. The shallow magma chamber provides magma through radial dykes and inclined sheets whereas the deeper magma reservoir provides primitive magma through regional dykes. Shallow magma chambers are the sources of the bimodal products of the central volcanoes as well as collapse calderas at the TVP while the deep-seated reservoir may be the source of monogenetic basaltic rocks at the periphery of the province. b) The simplified illustration of circular magma chamber at shallow depth d subject to magmatic excess pressure p_e. The maximum tensile stress σ_{max} occurs at the boundary at points c_1 and c_2 once the angle θ reaches a maximum. The tensile stress σ_b at a point b is equal to internal magmatic excess pressure p_e while at point a depends mainly on the radius r and depth d of the magma chamber (see text for more explanation) (modified from Gudmundsson, 2020).

The cross-cutting relationships indicate that many of the radial dykes were emplaced later than many or most of the inclined sheets (Fig. 5b). The inclined sheets, on average, may have been injected from deeper parts of the chamber and then less evolved than the radial dykes, many of which were most likely injected from the uppermost (more evolved) part of the chamber. The distribution of radial dykes and inclined sheets indicates the existence of two magma sources, either two magma chambers or two compartments within a stratified chamber. In the latter scenario, the compartments would be formed partly due to the difference between the density of felsic and mafic magma within the same magma chamber where the high density

magma would accumulate at deeper levels and the low density (light) magmas near the top of the chamber.

In the Toom central volcano there is a bimodal chemical distribution of rocks (Fig. 4b). The first generation is made of less evolved volcanic rocks (basaltic rocks) whereas the second generation is made up of more evolved volcanic rocks (rhyolite) (Vincent, 1970; Permenter and Oppenheimer, 2007; Deniel et al., 2015). At the contacts with the Tieroko pluton (Fig. 4a), the dips of the host rocks increase sharply

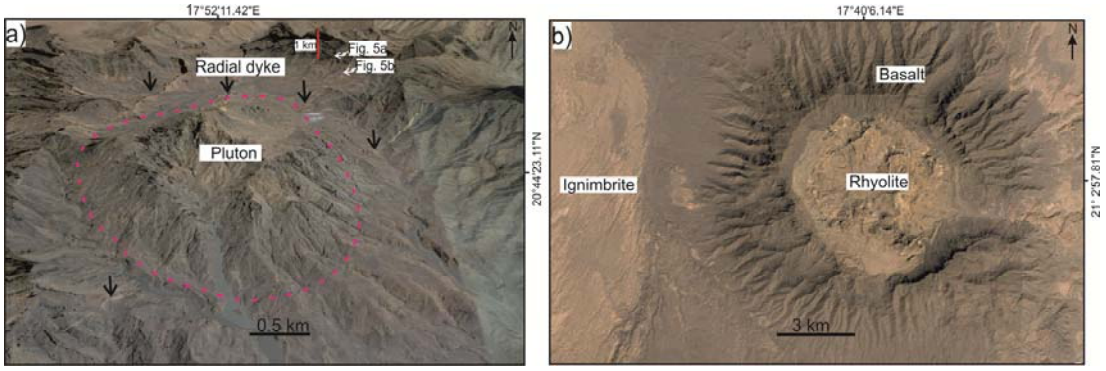

Figure 4. a) Satellite imagery (adapted from Google Earth) showing the deeply eroded Tieroko extinct central volcano. The black arrows indicate the radial dykes (lighter colour than the surroundings) that may have been injected from the uppermost part of the magma chamber. The exposed part of the chamber, a pluton, is at a depth few kilometres below the initial top of the associated volcano (cf. Deniel et al., 2015). The white arrows indicate the locations of Figures5a, b.. b) The composite central volcanoes of the TVP consist of two distinct volcanic phases. The first phase made up of basaltic lavas and emplaced around the margin while the second phase consists of rhyolite and erupted in the central part. The description and names are taken from Deniel et al.(2015).

from 10^{o} to as much as 20^{o}, suggesting that the pluton (a fossil magma chamber) generates space for itself partly through forceful intrusion, primarily by bending or uplift of the layers above and below.

4.2 Numerical models

We made many numerical models using the finite-element method (FEM) to study in detail stress fields associated with the magma chambers of the Tibesti Volcanic Province (TVP). The finite element method (FEM) is the most common technique for solving numerically differential equations (Henk et al., 2013; Hickey and Gottsmann, 2014). Numerical models based on the finite element method provide quantitative information on the local stresses around magma chambers. Such models

are of great help in improving our understanding the volcanotectonics of the TVP because local stress fields are known to control the emplacement of dykes and sheets (and associated eruptions), as well as the formation of collapse calderas. Comsol Multiphysics (5.2), a commercial multi-purpose software, is the finite element program used in this paper (www.comsol.com). More details on the standards modelling procedure can be found in Deb (2009).

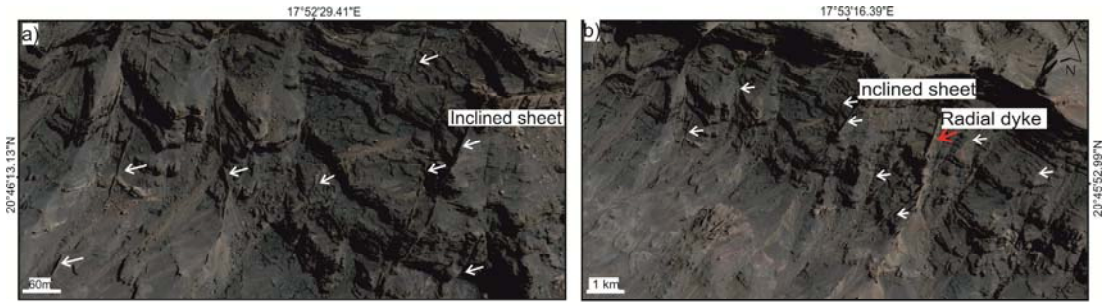

Figure 5. a) Swarms of inclined sheets, indicated by white arrows, in the eroded Tieroko extinct central volcano (located in Figure 4a). They appear basaltic and are mostly 0.5-3 m thick. b) Rhyolitic radial dyke (indicated by red arrow) cross-cutting the inclined sheet that may be assumed younger than basaltic inclined sheets (indicated by white arrows).

A magma chamber can be modelled as a finite size cavity in a three-dimensional model or as a hole in a two-dimensional model. The hole/cavity is modelled as filled with fluid under pressure when the chamber is active, but as an elastic inclusion when the chamber has become extinct (a pluton, a fossil chamber). Both active and extinct/fossil chambers concentrate stresses when loaded (Elshaafi and Gudmundsson, 2018; Gudmundsson, 2020). The active magma chamber may have a zero Young's modulus (if totally fluid) while the fossil magma chamber, a pluton, has normally a higher Young's modulus than the host rock.

Here we model the magma chamber as hole with diameter of 14 km and a top at 7 km depth. For the spherical chamber, this diameter is that of a circle, whereas for a sill-like chamber, this diameter is the lateral dimension of an oblate ellipsoid. The host rock is assumed to behave as elastic. The chamber is subject to magmatic excess pressure of 5 MPa as the only loading (Figs. 6a, 7a). From the definition of excess pressure given above, it follows that the effects of gravity are automatically taken into account.The plan-view cross-sectional area of the associated magma chamber at the TVP has been estimated from the geometry of the collapse calderas (cf. Marti et al., 1994; Marti and Gudmundsson, 2000; Acocella, 2007) (Table 1). Additionally, we estimated roughly the depth to the top of the magma chamber of the extinct

central volcano of Tieroko. We assume that this pluton represents the uppermost part of the extinct crustal magma chamber and take into account the erosion of several kilometres (Deniel et al., 2015). The results of numerical models are not very sensitive to the exact depth, however.

To simplify our models, we modelled the crust as a homogenous layer with a static Young's modulus for of 40 GPa corresponding to the average static Young's modulus for the upper crust (Wienecke and Stadtler, 2014; Elshaafi and Gudmundsson, 2017) and Poisson's ratio of 0.25– a very common values for rocks (Gudmundsson, 2020). Model parameters used in the present study are summarised in Table (2). The results in Figs. 6 b, c and 7b, c, show generated around the margins for both main shapes of magma chambers, that is, spherical and sill-like magma chambers. The local tensile stress σ_3 satisfies reach 8-10 MPa and, thereby, the condition for failure or rupture of magma chamber (Eq. 1) because the magnitude of tensile stress exceeds the tensile strength of the host rocks, which is most commonly 2-4 MPa (Amadei and Stephansson, 1997).

Dykes or inclined sheets are primarily extension fractures so that they follow the trajectories of the maximum compressive principal stress σ_1 (Figs 6d, 7d). Hence the models suggest the sheet intrusions central part of the chamber would tend to be vertical (radial dykes) but inclined sheets from the marginal parts. The modelling results are in agreement with field observations at the Tieroko central volcano (Figs. 4a, 5a, b). To test the effect of remote or regional stress field we made some additional numerical models with the same crustal properties, Young's modulus of 40 GPa and a Poisson's ratio of 0.25 as in the previous models. In these models, however, we use asymmetric regional tensile stress of 5 MPa, with a NE-SW direction, as the only loading (Fig. 8a). Again we use 5 MPa because the tensile strength of rocks is commonly around that value (Haimson and Rummel, 1982; Schultz, 1995; Amadei and Stephansson, 1997).

The results (Fig. 8b, c) show that the maximum tensile σ_3 and shear τ stresses concentrate above the top of the magma chamber rather than its margins and the trajectories of the maximum principal compressive stress σ_1 are generally vertical and favour the formation vertical dykes rather than inclined sheets (Fig. 8d). Similar results were obtained for a spherical chamber subject to external tension, but are not

shown here. Thus, the radial dykes and inclined sheets in the Tieroko centre volcano were most likely generated by local stress fields associated with a magma chamber that was subject to internal excess pressure rather than external tension. The latter, however, could be partly responsible for formation vertical dykes from the deeper magma reservoir rather than inclined sheets from the shallow crustal magma chamber. Our findings are in good agreement with field observations and modelling of deeply eroded, extinct central volcanoes in Iceland (Gudmundsson, 2020).

,

5 Mechanism of caldera collapse

Calderas are among the most important volcano-tectonic features of the TVP but are still poorly documented and modelled. A collapse caldera is generally defined as a depression, elliptical or circular in plan-view, with a diameter of 1 km or more and vertical displacement (subsidence) from a few hundred meters to 1-2 kilometres or more (Marti and Gudmundsson, 2000;Acocella et al., 2004; Acocella, 2007). Collapse frequently occurs along steep dip-slip ring-faults, so as to either inward-dipping (normal fault) or outward-dipping (reverse fault) (Fig. 9). Many ring-faults are used as magma conduits during collapse, thereby generating ring-dykes (Browning and Gudmundsson 2015). Caldera collapses can be subdivided into two groups based on the types of volcanoes in which they occur (Francis, 1993; Lipman, 2000; Radebaugh et al., 2001; Krassilnikov and Head, 2004; Cole et al., 2005). The first group consists of calderas in shield volcanoes (basaltic edifices) such as Hawaii and Galapagos and have common diameters of 6-7 km. The second group contains

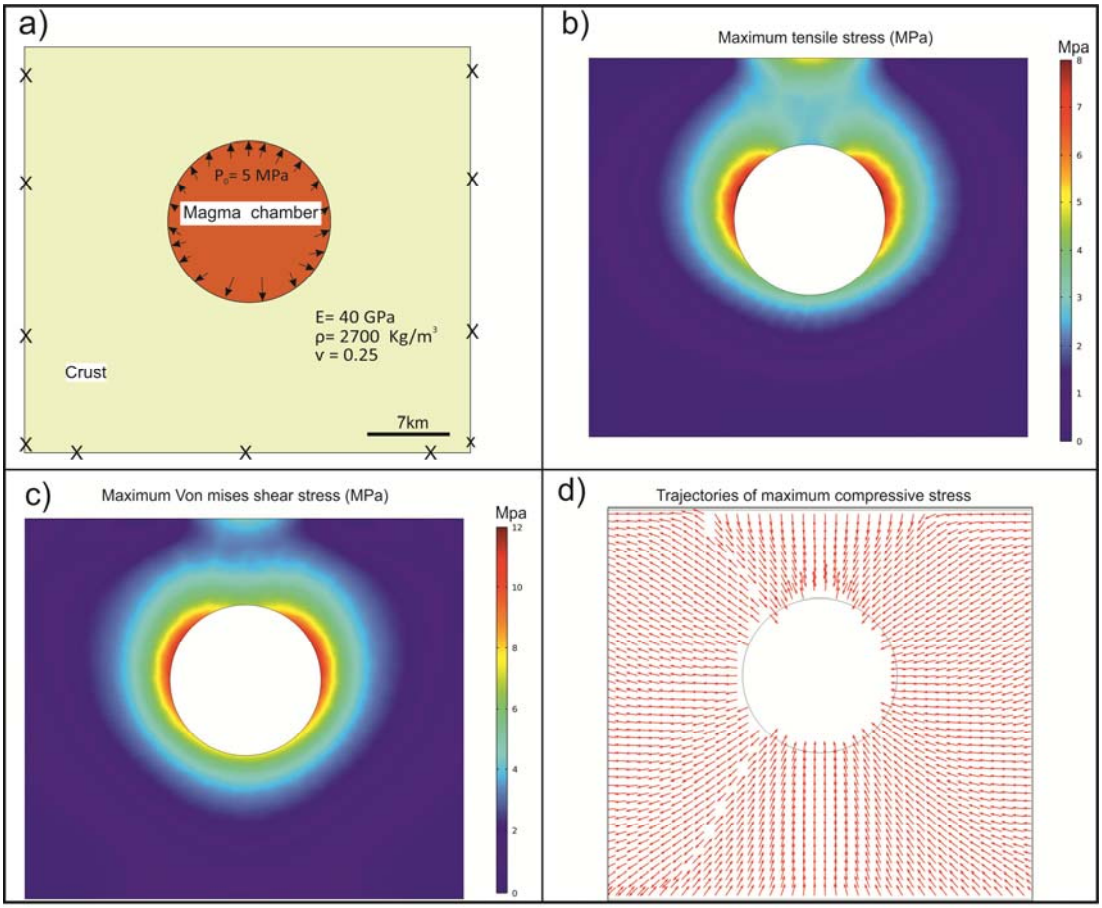

Figure 6. a) Model outline showing circular magma chamber with a top at depth 7 km and a diameter of 14 km subject to internal magmatic excess pressure of 5 MPa as the only loading. The model is fastened at the outer boundary using a fixed constraints to avoid any rigid body rotation or displacement. b) Colour contours showing the magnitude of the maximum principal tensile stress σ_3 ,and c) the von Mises shear stress in τ in mega-pascals. The maximum stresses occur at the boundary of the chamber and are consistent with the analytical model (Fig. 3b). d) The trajectories of the maximum principal compressive stress σ_1 which magma-driven fractures (dyke/inclined sheets) normally follow.

calderas that occur in composite volcanoes or stratovolcanoes and have common diameters of 18-19 km (Radebaugh et al., 2001). Three major collapse calderas, in addition to several small nested calderas, have been identified on the TVP. These major calderas have diameters of 12-16 km (Fig. 2). They are thus similar in size to typical calderas in the second group, but larger than typical calderas in the first group (Table 1). The calderas on the TVP have been partly filled with lava flows in their interiors and at their rims (the ring-fault) (Fig. 10 a, b), similar to that of many calderas worldwide.

While many different models have been suggested for explain the relationship between ring-faults and associated shallow crustal magma chambers into which the

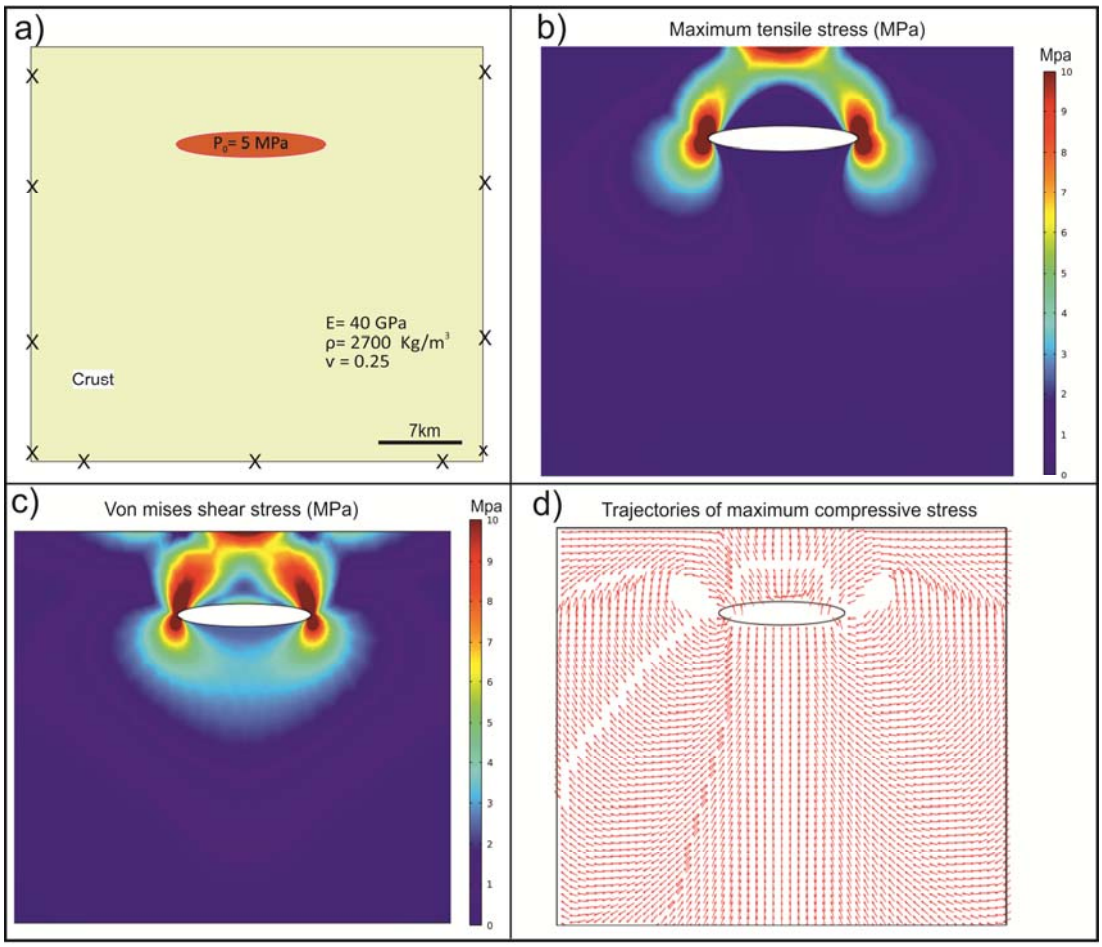

Figure 7. a) Model outline showing a sill-like magma chamber with a top at a depth of 7 km and with diameter of 14 km. The chamber is 2 km thick and subject to internal magmatic excess pressure of 5MPa as the only loading. The results of model yield similar results as for circular magma chamber (Fig. 6). b) The maximum tensile principal stress σ_3 and c)the maximum von Mises shear stress τ occur at lateral ends of the magma chamber and in the centre part of free surface. d) The trajectories of maximum principal compressive stress σ_1.

caldera piston-like block subsides (Walker, 1984, Marti et al., 1994; Burov and Guillou-Frottier, 1999; Acocella et al., 2004; Folch and Marti, 2004; Gray and Monaghan, 2005),rather little attempt has been made to clarify the exact mechanics of ring-fault formation. It is well known that a ring-fault must be generated before the piston-like caldera subsidence can take place. Ring-faults are commonly inward-dipping, that is, normal faults (Gudmundsson, 2016), as we infer for the ring-fault of the TVP, where the caldera subsidences helped generate ignimbrite volumes in excess of 100 km^3 for each individual caldera (Deniel et al., 2015; Table 1). Inward-dipping ring-faults can be generated when volcanic province containing volcano is subject to a slight doming or an extension, particularly in rift zones and in continental grabens. When the inward-dipping is close to vertical, a ring-dyke is

likely to propagate up the fault and the subsidence may squeeze out a large fraction of the magma in the chamber– a mechanism we propose for the large ignimbrite eruptions in the TVP.

It should be noted that collapse calderas are not always associated with large eruptions. Whether an eruption occurs during collapse, and the volume of the eruptive materials, depends largely on the dip of ring-fault and partly on the composition of the magma. Outward-dipping ring-faults encourage ring-dike fed eruptions, often large ones, whereas inward-dipping ring-faults may slip without any associated eruption (Gudmundsson, 2020).

It is well known that caldera-collapse conditions depend strongly on the shape of the magma chamber and the loading conditions, as well as Young's moduli of the host rocks (Gudmundsson, 2007). The geometry and size of a magma chamber generally changes during its evolution. Only specific shapes of magma chambers are favourable for formation collapse calderas, primarily oblate ellipsoidal or sill-like chambers, while others such as prolate ellipsoidal or spherical are unlikely to generate local stress field for the formation collapse calderas (Gudmundsson, 1998, 2007). Therefore the ordinary eruptions from chambers associated with collapse calderas, through radial dykes and inclined sheets, are many times more common than renewed slips on the existing ring-fault (Newall and Dzurisin, 1988; Gudmundsson, 2020). The stress field associated with various geometries of a magma chamber through its lifetime commonly favours the injections of inclined sheets and dykes whereas the stress a field favouring the formation or slip on the existing ring-fault is very rare. More specifically, for a ring-fault to form or slip, the shear stress τ and the near-surface tensile stress σ_3 must peak above the lateral margins of the magma chamber – a stress field that is rarely generated.

Caldera	Age (Ma)	Legth (km)	Width (km)	Maximum Depth (km)	Area (km^2)	Eruptive Volume (km^3)
Yirrigue	0.43	15.2	13.15	0.387	3223	150
Emi Koussi	2.4-1.3	12	12	0.356	2777	Unknown
Voon	7-5	15.8	13.6	0.308	2167	130

Table 1. The cross-sectional area, maximum depth, and eruptive material (area and volume) associated with each major collapse caldera of the TVP. The ages and eruptive volumes are taken from Deniel et al. (2015).

We made many numerical models on stress fields around magma chambers in order to clarify the condition for ring-fault formation using Comsol (www.comsol.com). In the first models presented here and discussed above the maximum surface tensile σ_3 and von Mises shear τ stresses are the result of excess magmatic pressures p_e (Figs. 6, 7) or external (asymmetric) tension, e.g. due to differential tensile loading or effects of transtension strike-slip loading (Fig. 8). In the models these stresses are mainly concentrated above the centre of magma chamber rather than its lateral edges and are accordingly not at a suitable location for ring-fault or ring-dyke formation while being favourable to radial dyke and inclined sheet injection.

We thus made additional models using the same crustal properties, Young's modulus of 40 GPa and a Poisson's ratio of 0.25 as in the previous models (Table 2), but different loading conditions. In these models there is a deep-seated magma reservoir with a width of 50 km located at the bottom of the crustal segment holding the shallow chamber. We use 10 MPa (Fig. 8a) for the excess pressure in a deep-seated source reservoir (Fig. 9), resulting in doming of an area much larger than that of the shallow chamber and then most likely to generate a collapse caldera (cf. Williams and McBirney, 1979; Lipman, 1984; Komuro, 1986; Marti and Gudmundsson, 2000). The primitive magma generated due to partial melting in the mantle ultimately accumulates at the crust-mantle boundary (Permenter and Oppenheimer, 2007, Lemnifi et al., 2019; Gudmundsson, 2020). For TVP we assume that the deep-seated magma reservoir is located at an average depth of 35 km, which generally corresponds to the boundary between the lower crust and upper mantle in the central and southern Libya (Ghanoush et al., 2014, Lemnifi et al., 2017). This depth is also consistent with depth of magma reservoir in the Al Haruj Volcanic Province (AHVP), central Libya (Peregi et al., 2003; Nixon et al., 2011; Lemnifi et al., 2019).

For the calderas in the area (Figs. 9, 10), the shallow magma chamber is modelled as elliptical in cross-section with a major axis of 14 km and at depth of 7 km (Fig. 11a). The models show that slight crustal doming due to pressure in the deep-seated reservoir results in the maximum tensile stress σ_3 at the margin of magma chamber

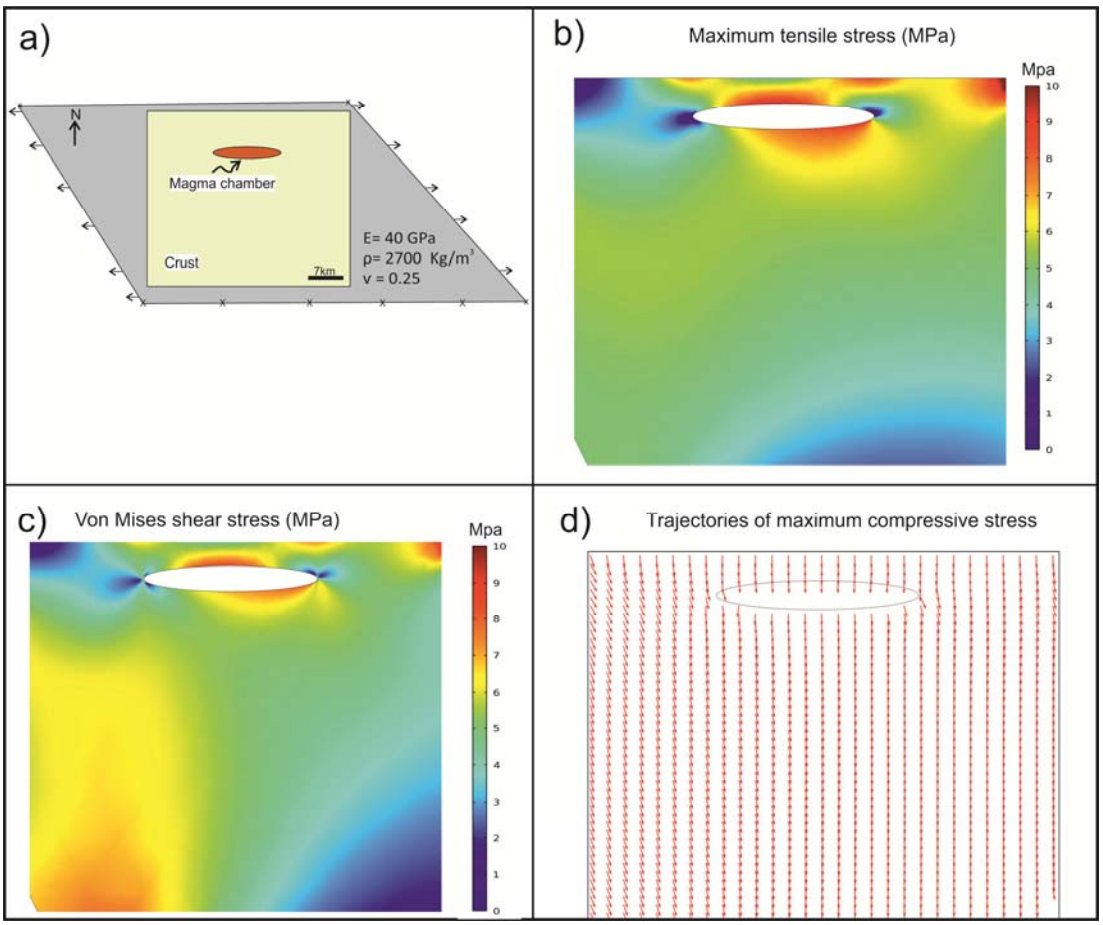

Figure 8. a) Model setup showing the sill-like magma chamber with a top at 7 km and 14 km wide. The chamber is 2 km thick and located in a homogeneous, isotropic crustal segment with stiffness of 40 GPa. Note the direction of tension applied to the model demonstrated by the arrows. The tension is 5 MPa and is the only loading. b) The maximum tensile stress σ_3 and c) the maximum von Mises shear stress τ occur at the top and bottom of the magma chamber rather than at the later ends. d) Trajectories of the maximum principal compressive stress σ_1.

reaching about 3.5 MPa (Fig. 11b, c) and generating two peaks of 5.5 MPa at the free surface above the margins of the chamber (Fig. 11b, d). Furthermore, the von Mises shear stress τ at the margin of the chamber reaches about 9 MPa while at the free surface above the chamber margin it peaks at about 4.5 MPa (Fig. 12a, c).

The shear strength τ_0 of most rocks has been estimated from stress drop of earthquakes as between 1 MPa to 12 MPa (occasionally as high as 30 MPa), and is commonly 3-6 MPa (Kanamori and Anderson, 1975; Kanamori, 1977), while the in situ tensile strength T_0 is mostly between 0.5 MPa and 6 MPa (occasionally, 9 MPa)

and mostly around 2-4 MPa (Amadei and Stephansson, 1997). Theoretical considerations indicate that the shear strength should be about twice the in-situ

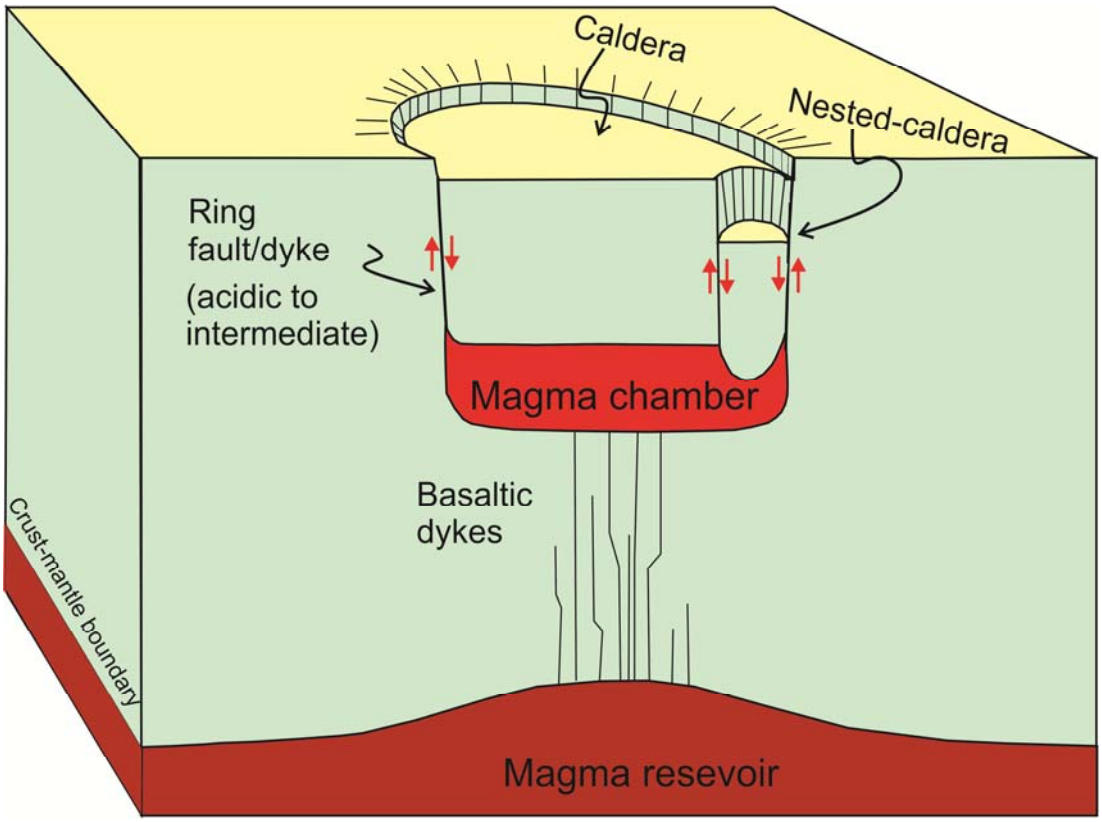

Figure 9. Schematic illustration of a nested collapse caldera. The cross-sectional area of the magma chamber can be inferred crudely from area of the caldera. Most collapse calderas occur when magma accumulates at the lower crust/mantle-crust boundary and causes doming of a much larger area than the lateral cross-sectional area of the shallow crustal magma chamber. The ring-fault slip plays a significant role in maintaining excess pressure and squeezing out magma during caldera collapse. Nested collapse calderas are common: for example, the Tou au Natron caldera within the larger Yirrigue caldera at the NE Tibesti Volcanic Province (Fig. 10a**).**

tensile strength, in general agreement with observations (Gudmundsson, 2020).In addition, the tensile T_0 and shear τ_0 strengths of the host rocks of magma chambers may be slightly reduced due to thermal effects of the active chamber (Browning et al., 2016). Based on these values for in-situ shear and tensile strengths, the numerical models presented above (Figs. 11 and 12) suggest that during slight doming the conditions for ring-fault initiation are satisfied. More specifically, the magnitudes of the maximum tensile σ_3 and shear τ stresses at the lateral ends of the magma

chamber and at that radial distance from the surface point above the centre of the chamber are similar to the typical in-situ range of tensile T_0 or shear strength τ_0 of ordinary rocks. These stresses are thus likely to trigger ring-fault initiation or slip on an existing ring-fault as well as the emplacement of ring-dykes from margins of the magma chamber.

6 Discussion

6.1 Magma supply by double magma sources and caldera collapse

The variety of volcanic products along the TVP, ranging from basaltic to acidic during the end of Miocene to late Pleistocene, indicates that the magma in this volcanic field is likely to be derived from a double magma chambers. By contrast, the volcanic provinces in Libya are likely to be supplied with magma from single magma reservoirs, presumably located at the crust-mantle boundary (cf. Peregi et al 2003; Less et al 2006; Nixon et al., 2011,Lemnifi et al., 2017; Ball et al., 2019). The more evolved acidic volcanic rocks (rhyolite, trachyte and ignimbrite, supplied by the shallow chamber) in the TVP are mostly concentrated in the central part of the province while the less evolved basaltic rocks are primarily distributed along its margins (Fig. 1b).

The shallow magma chamber presumably formed when some of dykes injected from the central part of the deeper magma reservoir became deflected into an initial sill within the upper part of the crust, due to abrupt changes in the mechanical properties and local stresses of the crustal rocks. Some of the primitive dykes continued to propagate directly to the surface and feed eruptions outside the shallow chamber. Field observations and numerical model results are generally in agreement with this assumption, where basaltic magma (scoria cones) can be observed around the periphery of the volcanic edifice while more evolved (rhyolite and ignimbrite) as well as some basalts are present mainly in the central part. In fact, similar distributions of eruptive products are well known and documented in other volcanic areas, such as the Ağrı Dağı volcanic field, eastern Turkey (Karaoğlu et al., 2016; 2017) and Iceland (Gudmundsson, 2020).

Model Parameter	Units	Value
Crustal Young's modulus	GPa	40
Crustal density	kg/m³	2700
Poisson's ratio		0.25
Excess magmatic pressure	MPa	5
Crustal thickness	km	35

Table 2. Model parameters used for the numerical models in the present paper.

Several of central volcanoes (composite volcanoes/stratovolcanoes) and collapse calderas of the TVP are poorly documented and understood, particularly as regards their relationship with volcano-tectonic forcing. These volcanism seems to be superimposed on the two preferential regional pre-existing lineaments where the central volcanoes (Yega, Oye and Toom) are well developed along the NE–SW trend (Deneil et al., 2015),while the collapse calderas (Voon, Emi Koussi and Yirrigue) are roughly along the NW–SE direction (Fig. 1b).We made two sets of numerical models in order to better understand the volcano-tectonic processes that led to the formation of volcanic edifices (8–5Ma) followed by caldera collapses (7–5 Ma to 0.43 Ma). The results of the first numerical models(Figs. 6-8) indicate that the local stress fields around magma chamber and on the free surface due to excess magmatic pressure p_0 or regional stress field are likely to encourage only the emplacement of dykes and inclined sheets and produced small range in eruptive volume, commonly between 0.01 $km^3$and 0.1km^3 (Karaoğlu et al., 2005; Gudmundsson, 2016). In addition, it is well-known that the geometry and size of magma chamber change considerably during its evolution and also the local stress field. Thus we infer that the cross-cutting between sheets at the Tieroko extinct central volcano is controlled by in situ stress field around chamber rather than regional stress field.

In the second set of numerical models (Figs. 11-12) we considered the effect of crustal doming due to an accumulation of magma in a deep-seated reservoir. The results of the second models indicate that slight doming at the bottom of lower crust results in local stresses that encourage initiation ring-faults at surface or at the shallow depths as well as injection of ring-dykes from the lateral ends of the shallow chamber. The resulting caldera collapses produced eruptive volumes as much as 100 km^3.

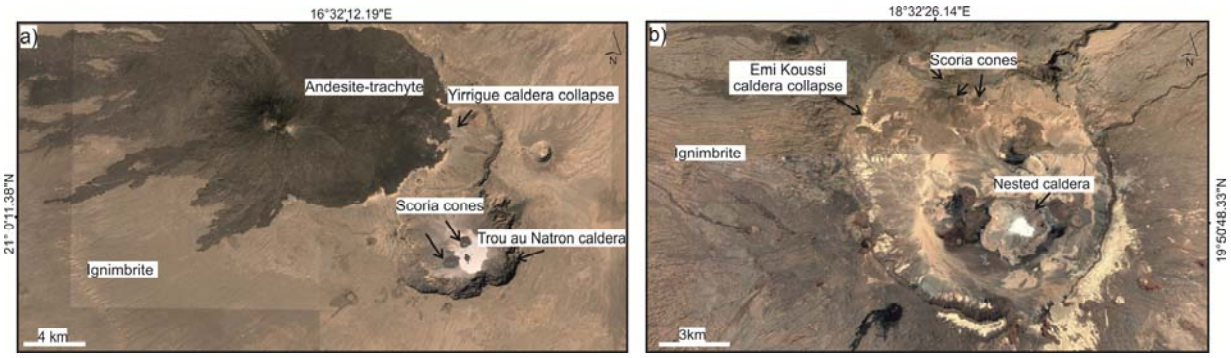

Figure 10. Satellite images (adapted from Google Earth) exhibit two main collapse calderas at the TVP. a) The Yirrigue caldera collapse (0.43Ma) is associated with the nested Trou au Natron caldera and followed by eruptions of andesitic-trachyte (100 ka) materials at its margin. Some of the ring-faults/ring-dykes of the caldera may be buried by the subsequently formed post-caldera Tousside complex (Daniel et al., 2015).b) the Emi Koussi caldera collapse (2.4–1.3 Ma) associated with a nested caldera in the central part and was followed by the formation of scoria cones along its margin and in the central part as well. Ignimbrites erupted from both calderas exceed volumes of 100 km^3.

6.2 Caldera collapse and new magma chambers

The rough elliptical surface expressions of the distribution of scoria cones on the TVP may be taken as an indication of a roughly elliptical geometry of the magma reservoir beneath this volcanic region (Fig. 13a). This follows from the observations that volcanic fields and volcanic systems tend to reflect the plan-view geometries of the source reservoirs. Hence, the long axis of the deeper reservoir may beroughly 365 km while its short axis is crudely193 km (Fig. 13a). For comparison, the long axis of collapse calderas at the TVP is 12-16 km (Table 1). Thus the doming area at the lower crust is very much larger than the crustal magma chamber and most likely played a major role in the formation of the collapse caldera (Williams and McBirney, 1979; Lipman, 1984; Komuro, 1986, Marti and Gudmundsson, 2000).

The late Miocene uplift in the whole western part of the Sirt Basin, central Libya, is confirmed by the burial history of oil wells (QQQ1-11; aa1-11), situated at the western margin of the Sirt Basin (Gumati and Schamel, 1988; Abadi et al., 2008). Also, the high degree of thermal maturity of shallow sediments indicates that up to several kilometres of a sedimentary sequence was uplifted and eroded during the late Miocene in the whole western part of the Sirt Basin (Gumati and Schamel, 1988;

Abadi et al., 2008). This regional uplift seems to have impacted on the whole Tibesti–Gharyan volcanic provinces. As a result the crustal doming during the end of

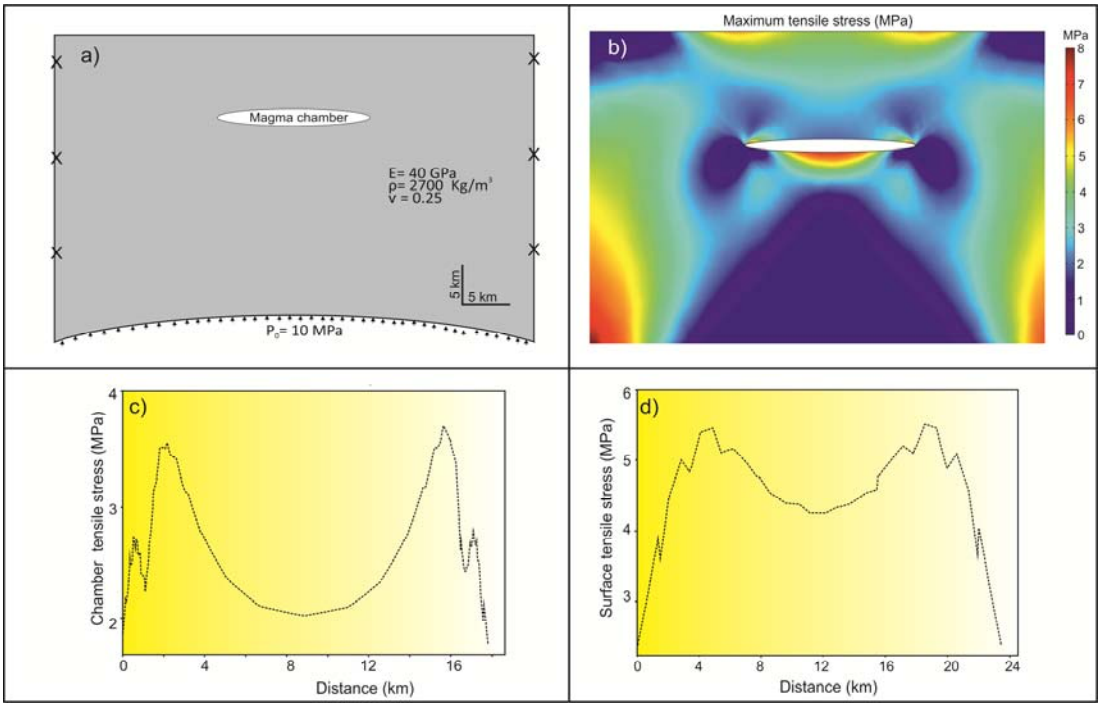

Figure 11. a) . Model outline showing ellipse (sill-like) magma chamber with a top at 7 km, 14 km wide, and a thickness 2 km in a homogeneous, isotropic crustal segment with an average Young's modulus of 40 GPa. The crustal segment is 35 km thick and 50 km wide and subject to(doming) pressure, p_e of 10 MPa at its lower margin (bottom). b) The result of modelling showing the magnitude of the maximum principal tensile stress σ_3. c) Graph showing the maximum principal tensile stress σ_3 at the upper boundary of the magma chamber. d) Graph showing the maximum principal tensile stress σ_3 at the free surface.

Miocene and increased melt migration into the magma reservoirs beneath most of the Tibesti–Gharyan volcanic provinces in general and the TVP in particular might have led to elongated magma reservoirs and accumulation of magma at the crust-mantle boundary. Therefore, the magmatic excess pressure in the magma reservoir at the crust-mantle boundary may have caused doming of the crustal segment hosting the three major collapse calderas. Accordingly, the collapse calderas on the TVP can be investigated in the light of the conceptual model is given by Marti and Gudmundsson (2000). This model indicates how and under what stress condition overlapping collapse calderas can be generated by magma migration. In addition, this model is applicable for explaining magma chamber migration in regions where

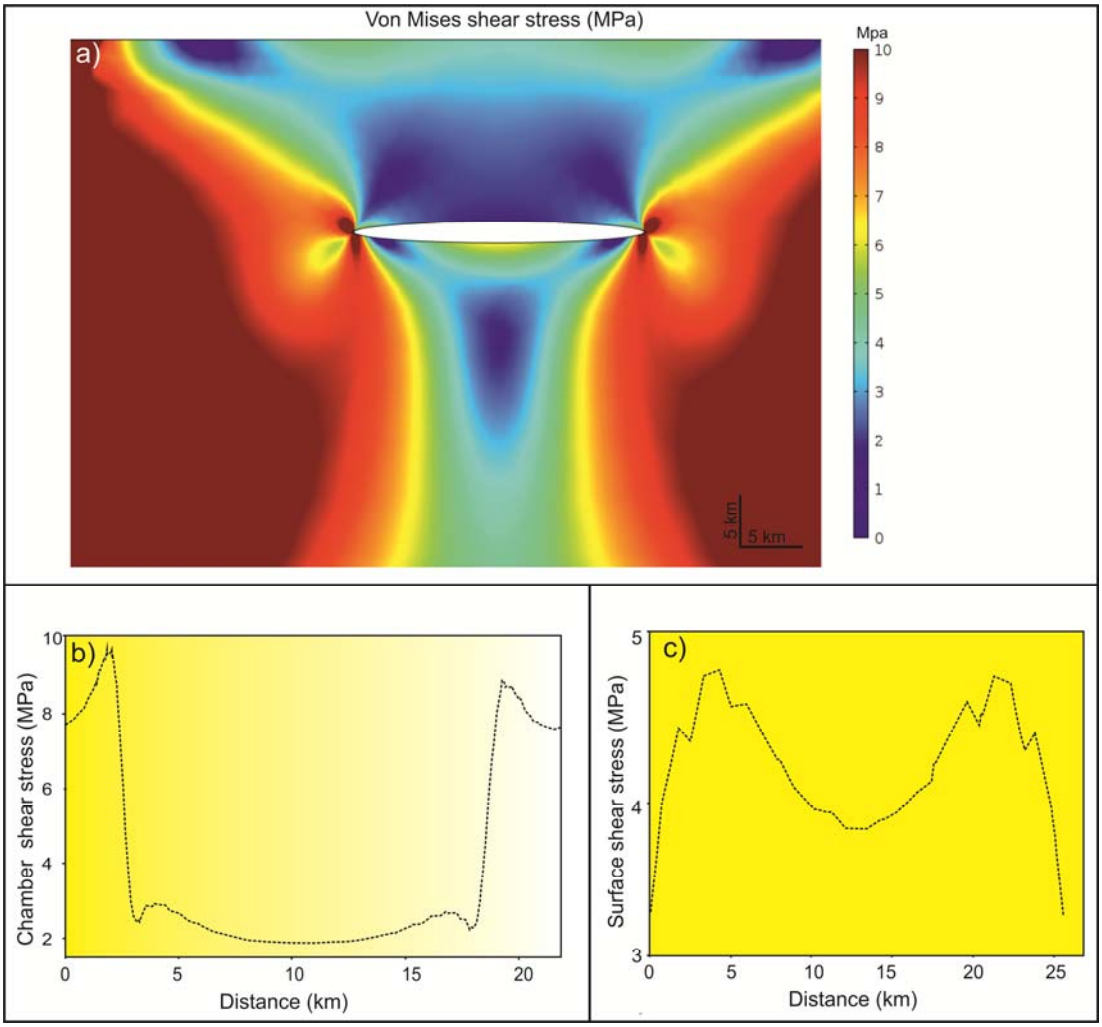

Figure 12. a) Same model as in Fig. 11 but here showing. a) the magnitude (contours) of the von Mises shear stress τ around magma chamber and at the free surface in mega-pascals, b) the variation in the von Mises shear stress τ at the upper boundary of the magma chamber, and c) the variation in the von Mises shear stress τ at the free surface.

late or continent is very slowly drifting such as African plate (i.e. Burke 1996; Begg et al., 2009), because bending tensile stress σ_3 controls the location of dyke injection frequently for a significant period rather than a fast drifting plate.

As a result of magma accumulation at the bottom of the crust and doming, the central lower part of the crustal segment hosting the collapse calderas becomes subject to compressive stress while the lateral ends are subject to tensile stress (Fig. 13b). Because of the compressive stress above the central deeper magma reservoir, it may be difficult for dykes to penetrate and replenish the old shallow magma chamber (cf. Marti and Gudmundsson, 2000). By contrast, the tensile stress σ_3 in the

crustal segment above the lateral sides of the deeper magma reservoirs are likely to encourage dyke injections. Each individual collapse caldera on the TVP appears to be formed at the end of a cycle. Once the magma chamber was full-grown and had assembled large volumes of potential ignimbrite magma (gas-rich acid magma), the tectonic-volcanic forcing (slip of the ring-faults) may have led to the subsidence roof of the associated felsic magma chamber and produced huge eruptive materials (ignimbrites). The tensile stress σ_3 in the lower crust is most likely favourable to dyke emplacement and new magma chamber formation to either side of the old magma chamber and hence magma chamber migration rather than replenishment of the old magma chamber (cf. Marti and Gudmundsson, 2000). The migration of the magma chambers of the TVP is supported by field-relations and geochronological data (Deniel et al., 2015) (Fig. 13b).

The first caldera collapse (Voon caldera) occurred at the end of Miocene (7-5Ma) and may have been simultaneous with the first volcanic phase at the Al Haruj Volcanic Province (AHVP) (7–3.6 Ma) (Less et al., 2006, Bardintzeff et al. 2012). The local stress field around the deeper magma reservoir, following the Voon caldera collapse may have made it difficult for dykes to feed the Voon chamber (old chamber) while the stress field was suitable for injection of dykes from margins of the deeper reservoir. Thus the new magma chamber may have been created in the northwestern part of the TVP (Emi Koussi caldera, 2.4–1.3 Ma) (Figs.2, 13b). This new magma chamber seems to be taken around 2.5 Ma based on the available geochronological data (Deneil et al., 2015). Subsequently, however, after the collapse of the second magma chamber, the new and third magma chamber (Yirrigue caldera, 0.43 Ma) may have been formed in the northwestern part of the TVP. This chamber lasted around 1 Ma and developed rhyolitic magma from primitive magma.. Most of the basaltic lavas are distributed along rims of calderas (e.g., Fig. 10a) due to most likely basaltic magma used pre-existing ring-faults/ring-dykes as conduits (cf. Browning and Gudmundsson, 2015; Elshaafi and Gudmundsson, 2016). Nevertheless, geophysical and volcanology investigations will certainly be needed to further establish the details of the TVP development through better constraints on the shallow magma chambers and volcano-tectonic forcing and volcano-tectonic forcing.

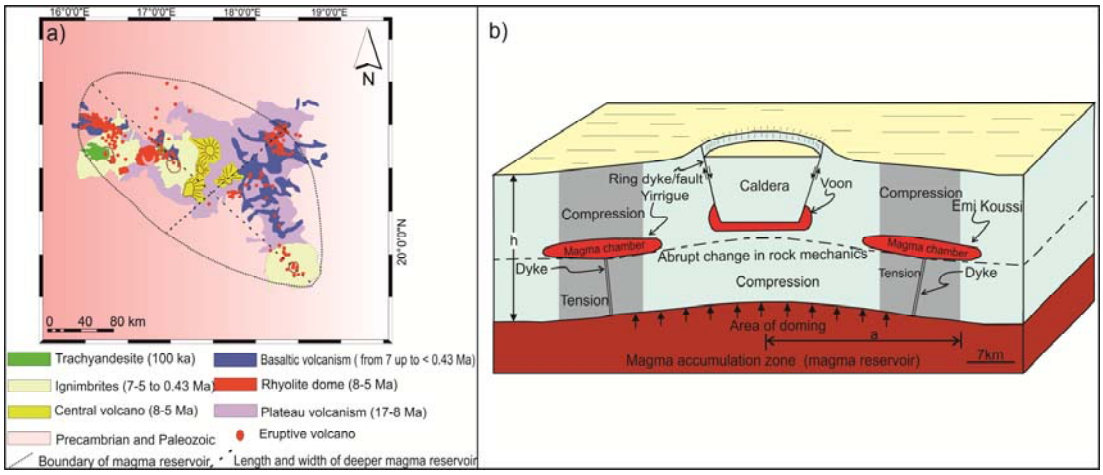

Figure 13. a) Simplified geological map of the TVP showing the areal distribution of the scoria cones (red spots) (7-0.43 Ma) which may be used to estimate crudely the dimensions of deep-seated magma reservoir. b) Conceptual model illustrating the mechanism of migrating collapse calderas and the generation of new magma chambers (modified from Marti and Gudmundsson, 2000). This model fits reasonably well with the mechanism of collapse calderas at the TVP. The compressive stress just above the deeper magma reservoir makes it difficult for dykes to feed the Voon magma chamber while tensile stresses at the lateral ends of the deeper magma reservoir may have encouraged dyke propagation to form the Emi Koussi magma chamber.. After the destruction of Emi Koussi magma chamber, the local stress field may have been suitable for the formation of the third new magma chamber (Yirrigue magma chamber).. Here a is the radius of the deeper magma reservoir and h is the thickness of the crustal segment (modified from Marti and Gudmundsson, 2000).

7. Conclusions

In conclusion, the main results of the present study may be summarised as follows:

- The volcanic products along the Tibesti Volcanic Province (TVP) range from under-saturation basaltic rocks to over-saturation acidic rocks indicate that magmas were erupted from double magma sources. The rocks range in age from late Miocene to end of Pleistocene.
- Each double magma source consists of a shallow magma chamber in the upper crust and a deep-seated and much larger magma reservoir at the boundary between the crust and the upper mantle. The reservoir supplies magma to the chamber, which in turn produces a central volcano (composite volcano/stratovolcano).
- Field observations and numerical model results suggest that basaltic magma at the margins of the TVP may be injected directly from the deeper magma

reservoir at the lower crust whilst the more evolved rhyolite and ignimbrite most likely were derived from shallow crustal magma chamber.

- The evolution of the TVP is characterised by, first, a period during which the central volcanoes formed (8-5 Ma), and subsequently and period of collapse-caldera formation(5-0.43 Ma).The collapse calderas produced large-volume (>100 km^3) ignimbrite units.
- The piston-like subsidence during caldera collapse maintains the magmatic excess pressure in the magma chamber for a much longer time than in an ordinary eruption, thereby squeezing out an extraordinarily large fraction of the magma in the chamber, possibly most of its content. By contrast, in an ordinary eruption the excess magmatic pressure in the magma reservoir decreases rapidly so that only about 0.1% of the (basaltic) magma flows out of the reservoir during an eruption.

Acknowledgements

We thank Thorvaldur Thordarson for comments on an earlier version of the manuscript and the journal reviewers and the editor Irina Artemieva for many helpful comments on the present version.

References

Abadi, A., van Wees, J., van Dijk, P., Cloetingh, S., 2008. Tectonics and subsidence evolution of the Sirt Basin, Libya. AAPG Bulletin, 92, 993-1027.

Abdunaser, K., McCaffrey, K., 2014. Rift architecture and evolution: the Sirt Basin, Libya: the influence of basement fabrics and oblique tectonics. Journal of African Earth Sciences, 100, 203–226.

Acocella, V., 2007. Understanding caldera structure and development: and overview of analogue models compared to natural calderas. Earth-Science Reviews, 85, 125–160.

Acocella, V., Funiciello, R., Marotta, E., Orsi, G., de Vita, S. 2004. The role of extensional structures in experimental calderas and resurgence. Journal of Volcanology and Geothermal Research, 129, 199–217.

Ade-Hall, M., Reynolds, H., Dagley, P., Musset, G., Hubbard, B., Klitzsch, E. 1974. Geophysical studies of North African Cenozoic volcanic areas Al Haruj Al– Assuad, Libya. Canadian Journal of Earth Science, 11, 998-1006.

Amadei, B., Stephansson, O., 1997. Rock Stress and its Measurement. Chapman & Hall, London.

Ball, P., White, N., Masoud, A., Nixon, S., Hoggard, M., Maclennan, J.,Stuart, F., Oppenheimer, C., Kropelin, S., 2019. Quantifying Asthenosphericand Lithospheric Controls on Mafic Magmatism Across North Africa. Geochemistry. Geophysics, Geosystems-AGU Publications.

Bardintzeff, J., Deniel, H. Guillou, B. Platevoet, P. Télouk, Oun, K., 2012. Miocene to recent alkaline volcanism between Al Haruj and Waw an Namous (southern Libya) Int. Journal of African Earth Sciences, 101, 1047–1063.

Begg, G. Griffin, W., Natapov, L., O'Reilly, S., Grand, S., O'Neill, C., Hronsky, J., Djomani, Y., Swain, C., Deen, T., Bowden, P., 2009. The lithospheric architecture of Africa: Seismic tomography, mantle petrology, and tectonic evolution. Geosphere, Geological Society of America. 5 23–50.

Browning, J., Gudmundsson, A., 2015. Caldera faults capture and deflect inclined sheets: an alternative mechanism of ring dike formation. Bulletin of Volcanology, 77: 4DOI 10.1007/s00445-014-0889-4.

Browning, J., Meredith, P., Gudmundsson, A. 20016. Cooling-dominated cracking in thermally stressed volcanic rocks. Geophysical Research Letters 43, doi:10.1002/2016GL070532

Burke, K., 1996. The African plate, South African. The Journal of Geology. 99, 341–409.

Burov, E., Guillou-Frottier, L., 1999. Thermomechanical behaviour of large ash flow calderas. Journal of Geophysical Research, 104, 23081–23109.

Busrewil, M. Oun, K., 1991. Geochemistry ofthe Tertiary alkaline rocks of Jabal al Hasawinah, west central Libya. Third Symposium on the Geologyof Libya, (eds. M.J. Salem and M.T. Busrewil and A.M. Ben Ashour), Elsevier, Amsterdam,7, 2587–2598.

Chen N., Dong J. Chen, J., Dong C., Shen, Z., 2014. Geometry and emplacement of the Late Cretaceous mafic dyke swarms on the islands in Zhejiang Province, Southeast China: Insights from high-resolution satellite images, Journal of Asian Earth Sciences, 7, 302–311.

Cole, J., Milner, D., Spinks, K. 2005. Calderas and caldera structures: a review. Earth-Science Reviews, 69, 1-26.

Cloetingh, S., Van Wees, J., 2005. Strength reversal in Europe's intraplate lithosphere: Transition from basin inversion to lithospheric folding: Geology, 33, 285–288.

Dahm, T., 2000. Numerical simulations of the propagation path and the arrest of fluid-filled fractures. Geophysical Journal International, 141, 623-638.

Deb, D.,2009. Finite Element Method, (Concepts and Applications in Geomchanics). New Delhi. 2nd edition, p. 269.

Deniel, C., Vincent, P., Beauvilain, A., Gourgaud, A. 2015. The Cenozoic volcanic province of Tibesti (Sahara of Chad):major units, chronology, and structural features. Bulletin of Volcanology, 77, doi.org/10.1007/s00445-015-0955-6

Drury, S., 2001. Image Interpretation in Geology. Blackwell Science, Nelson Thornes,UK, p. 290.

Ebinger, C., Sleep N.1998. Cenozoic magmatism throughout East Africa resulting from impact of a single plume. Nature, 395, 1788–1791.

El–Makhrouf, A. 1988. Tectonic interpretation of Jabal Eghei area and its regional application to Tibesti orogenic belt, South Central Libya. Journal of African Earth Sciences, 7. 945–967.

Elshaafi, A., Gudmundsson, A., 2018. Mechanical interaction between volcanic systems inLibya. Tectonophysics 722, 549–565. https://doi.org/10.1016/j.tecto.2016.

Elshaafi, A., Gudmundsson, A., 2017. Distribution and size of lava shields on the Al haruj al Aswad and the Al haruj al abyad volcanic systems, Central Libya. Journal of Volcanology and Geothermal Research. Res. 338, 1–17.

Elshaafi, A., Gudmundsson, A., 2016. Volcano-tectonics of the Al Haruj Volcanic Province, Central Libya, Journal of Volcanology and Geothermal Research. 325, 189–202.

Folch, A., Marti, J., 2004. Geometrical and mechanical constraints on the formation of ring-fault calderas. Earth and Planetary Science Letters, 221, 215–225.

Francis, P., 1993. Volcanoes: a Planetary Perspective. Oxford University Press, Oxford.

Lipman, P.W. 2000. Calderas. In: Sigurdsson, H. (ed) Encyclopedia of Volcanoes. Academic Press, San Francisco, 643–662.

Ghanoush, H., Imber, J., McCaffrey, K., 2014. Cenozoic Subsidence and Lithospheric Stretching Deformation of the Ajdabiya Trough Area, Northeast Sirt Basin, Libya. AAPG 2014 Annual Convention and Exhibition, Houston, Texas.

Goudarzi, G., 1980. Structure – Libya. In : The Geology of Libya (eds.) Salem, M. J., and Busrewil, M. T., London Academic press, 3, 879– 892.

Gourgaud, A. Vincent, P. 2004. Petrology of two continental alkaline intraplate series at Emi Koussi volcano, Tibesti, Chad. Journal of Volcanology and Geothermal Research, 129, 261–290.

Gray, J., Monaghan, J., 2004. Numerical modelling of stress fields and fracture around magma chambers. Journal of Volcanology and Geothermal Research, 135, 259–283.

Gudmundsson, A., 1998. Formation and development of normal-fault calderas and the initiation of large explosive eruptions. Bulletin of Volcanology, 60, 160–170.

Gudmundsson, A., 2007. Conceptual and numerical models of ring-fault formation. Journal of Volcanology and Geothermal Research, 164, 142–160.

Gudmundsson, A., 2016. The mechanics of large eruptions. Earth-Science Reviews, 163, 72–93.

Gudmundsson, A., 2020. Volcanotectonics: Understanding the Structure, Deformation and Dynamics of Volcanoes. Cambridge University Press, Cambridge.

Gumati, Y., Schamel, S., 1988. Therma maturation history of the Sirte Basin, Libya: Journal of Petroleum Geology, 11, 205–218.

Haimson, B. Rummel, F., 1982. Hydrofracturing stress measurements in the Iceland research drilling project drill hole at Reydarfjordur, Iceland. Journal of Geophysical Research, 87, 6631–6649.

Henk, A., Fischer, K., Kromuller, K., Wanger, D., Winter, I., 2013.Prediction of Tectonic Stresses and Fracture Networks with Geomechanical Reservoir Models. DGMK-Research Report 721. German Society for Petroleum and Coal Science and Technology, p. 216.

Hickey, J., Gottsmann, J., 2014. Benchmarking and developing numerical Finite Element models of volcanic deformation. Journal of Volcanology and Geothermal Research, 280, 126–130.

Kanamori, H., 1977. The energy release in great earthquakes. Journal of Geophysical Research, 82, 2981–2987.

Kanamori, H., Anderson, D., 1975. Theoretical basis for some empirical relations in seismology. Bulletin of the Seismological Society of America, 65, 1073-1095.

Karaoğlu, Ö. Özdemir, Y., Tolluoğlu, AÜ., Karabıyıkoğlu, M., Köse, O., Froger, JL. 2005. Stratigraphy of the volcanic products around Nemrut Caldera: implications for reconstruction of the Caldera Formation. Turkish Journal of Earth Sciences, 14, 123–143.

Karaoğlu, Ö., Browning, J., Bazargan, M., Gudmundsson, A..2016. Numerical modelling of triple-junction tectonics at Karlıova, Eastern Turkey, with implications for regional magma transport. Earth and Planetary Science Letters, 452, 152–170.

Karaoğlu, O. Elshaafi, A., Salah, M., Browning, J., Gudmundsson, A., 2017. Large-volume lava flows fed by a deep magmatic reservoir atAğrı Dağı (Ararat) volcano, Eastern Turkey. Bulletin of Volcanology. 1–16.

Karlstrom, L., Dufek, J., Manga, M., 2010. Magma chamber stability in arc and continental crust. Journal of Volcanology and Geothermal Research, 190, 249-270.

Karlstrom, L., Paterson, S.R., Jellinek, A. M., 2017. A reverse energy cascade for crustal magma transport. Nature Geoscience, 10, 604-608.

Keppie, J., Dostal, J., Murphy, J., 2011. Complex geometry of the Cenozoic magma plumbing system in the central Sahara, NW Africa. International Geology Review. 53, 1576-1592.

Klitzch, E., 2000. The structural development of the Murzuq and Kufra basins significance for oil and mineral exploration, In: Sola, M. A. and Worsley, D. (Ed.). Geological exploration of the Murzuq basin. Elsevier, Amsterdam, 143-150.

Komuro, H., 1986. Experiments on cauldron formation: a polygonal cauldron and ring fractures. Journal of Volcanology and Geothermal Research. 31, 139–149.

Krassilnikov, S., Head, W., 2004. Calderas on Venus and Earth: comparison and models of formation. Lunar and Planetary Science, 35, 1531.

Kusumoto, S., Geshi, N., Gudmundsson, A., 2013. Aspect ratios and magma overpressures of non-feeder dikes observed in the Miyake-jima volcano (Japan), and fracture toughness of its upper part. Geophysical Research Letters, 40, 1–5, http://dx.doi.org/10.1002/grl.50284.

Lemnifi, A., Browning, J., Elshaafi, A., Aouad, N., Yu, Y., 2019.Receiver function imaging of mantle transition zone discontinuities and the origin of volcanism beneath Libya.Journal of Geodynamics. Doi.org/10.1016/j.jog.2019.01.009

Lemnifi, A., Elshaafi, A., Browning, J., El Ebadi, S., Gudmundsson, A., 2017. Crustal thickness beneath Libya and the origin of partial melt beneath AS Sawda Volcanic Province from receiver-function constraints. Journal of Geophysical Research Solid Earth. , DOI: 10.1002/2017JB014291.

Less, G., Turki, S. , Suwesi, S., Peregi, L. , Koloszar, L., Kalmar, J., Sherif, K., Csaszar, G., Gulasci, Z., Dalum, H., Al Tajuri, A., 2006. Explanatory Booklet. Geological Map of Libya 1 : 250.000. Sheet : Waw Al Kabir NG 33- 12. Industrial Research Centre, p. 295.

Liégeois J., Benhallou, A., Azzouni-Sekkal, A., Yahiaoui, R., Bonin, B. 2005. The Hoggar swell and volcanism: reactivation of the Precambrian

Tuareg shield during Alpine convergence and West African Cenozoic volcanism. In: Foulger GR, Natland JH, Presnall DC, Anderson DL (eds) Plates, Plumes, and Paradigms, Special Papers - Geological Society of America, 388, 379–400.

Lipman, P. 1984. The roots of ash flow calderas in western North America: windows into the tops of granitic batholiths. Journal of Geophysical Research, 89, 8801–8841.

Maccaferri, F., Bonafede, M., Rivalta, E., 2011. A quantitative study of the mechanisms governing dike propagation, dike arrest and sill formation. Journal of Volcanology and Geothermal Research, 208, 39-50.

Malin, M. 1977. Comparison of volcanic features of Elysium (Mars) and Tibesti (Earth). Geological Society of America Bulletin, 88, 908–919.

Marti, J., Ablay, G., Reshaw, T., Sparks, J. 1994. Experimental studies of collapse calderas. Geological Society, London, Special Publications, 151, 919–929.

Marti, J., Gudmundsson, A. 2000. The Las CanÄadas caldera (Tenerife, Canary Islands): an overlapping collapse caldera generated bymagma-chamber migration. Journal of Volcanology and Geothermal Research, 103, 161–173.

Mohamed, M., 2014. Composition and age of Cenozoic volcanism in Libya. PhD thesis. University of Glasgow. Glasgow Theses Service.

Newhall, C., Dzurisin, D., 1988. Historical Unrest of Large Calderas of the World. U.S. Geological Survey Bulletin, 2, p. 1108.

Nixon, S., Maclennan, J., White, N., 2011. Intra-plate magmatism of the Al Haruj Volcanic Field, Libya. Goldschmidt Conference Abstracts.

Peregi, Z., Less, G., Konrad, G., Fodor, L., Gulacsi, Z., Gyalog, L., Turki, S., Suwesi, S., Sherif, Kh., Dalub, H., 2003. Explanatory Booklet. Geological Map of Libya 1: 250.000. Sheet: Al Haruj Al Abyad NG 33-8. Industrial Research Centre, Tripoli, p. 248.

Permenter, J., Oppenheimer, C.2007. Volcanoes of the Tibesti massif (Chad, northern Africa). Bulletin of Volcanology, 69, 609–626.

Pinel, V., Jaupart, C., 2004. Magma storage and horizontal dyke injection beneath a volcanic edifice. Earth and Planetary Science Letters, 221, 245-262.

Radebaugh, J., Keszthelyi, L.P., McEwen, A.S., Turtle, E.P., Jaeger, W., Milazzo, M., 2001. Paterae on Io: a new type of volcanic caldera? Journal of Geophysical Research, 106, 33005-33020.

Radivojević, M., Toljić, M., Turki, S., Bojić, Z., Šarić, K., Cvetković, V., 2015. Neogene to Quaternary basalts of the Jabal Eghei (Nuqay) area (south Libya): Two distinct volcanic events or continuous volcanism with gradual shift in magma composition? Journal of Volcanology and Geothermal Research, 293, 57–74.

Rajesh, M., 2004. Application of remote sensing and GIS in mineral resource mapping an overview. Journal of Mineralogical and Petrological Sciences, 99, 83–103.

Rivalta, E., Taisne, B., Bunger, A.P., Katz, R.F, 2015. A review of mechanical models of dike propagation: schools of thought, results and future directions. Tectonophysics, 638, 1-42.

Schäfer K, Kraft K., Häusler, H., Erdmann, J. 1980. In situ stresses and palaeostresses in Libya. In: Salem MJ, Busrewil MT (eds) The geology of Libya. Academic Press, London, 3, 907–922.

Tibaldi, A., 2015. Structure of volcano plumbing systems: A review of multi-parametric effects. Journal of Volcanology and Geothermal Research, 298, 85–135. http://dx.doi.org/10.1016/j.jvolgeores.2015.03.023.

Townsend, M., Pollard, D.D., Smith, R., 2017. Mechanical models for dikes: a third school of thought. Tectonophysics, 703-704, 98-118.

Upton, B., 2004. Volcanoes and the Making of Scotland. Dunedin Acad. Press, Edinburgh.

Vail, J., 1971. Dikes swarms and volcanic activity in Northeastern Africa. In : (ed.) Gray, C. Faculty of Science University of Libya, Tripoli. 341–47.

Vincent, P.1960. Dynamismes et structures des volcans rhyolitiques du Tibesti occidental et central. Rev Geogr Phys Geol 2, 229–237.

Vincent, P.1963. Les volcans tertiaires et quaternaires du Tibesti occidental et central (Sahara du Tchad). Mémoires BRGM 23. Thesis 1st part, University of Paris.

Vincent P. 1970. The evolution of the Tibesti volcanic province, eastern Sahara. In: Clifford TN, Gass IG (eds) African magmatism and tectonics. Oliver and Boyd, Edinburgh, 301–319.

Wacrenier P, Hudeley H, Vincent P. 1958. Notice explicative de la carte géologique provisoire du Borkou-Ennedi-Tibesti au 1:1,000,000e. Direction des mines et de la géologie AEF, Brazaville.

Walker, G., 1984. Downsag calderas, ring faults, caldera sizes, and incremental caldera growth. Journal of Geophysical Research, 89, 8407–8416.

Wienecke, S., Stadtler, C., 2014. Asep+d method: identifying anomalous areas of the earth's lower crust, Publication number EP 2791713 A1, Patents.

Williams, H., McBirney, A., 1979. Volcanology. W.H. Freeman, New York.

Wilson, M., Guiraud., R., 1998. Late Permian to Recent magmatic activity on the African-Arabian margin of Tethys, in D. S. Macgregor, R. T. J. Moody, and D. D. Clark-Lowes, eds., Petroleum geology of North Africa: Geological Society (London) Special Publication, 132, 231–263.

Woller, F., Fediuk, F. 1980. Volcanic rocks of Jabal as Sawda. In: Salem, M.J., Busrewil,M.T. (Eds.), The Geology of Libya III. Academic Press, London, 3 1081–1093.